https://doi.org/10.5194/egusphere-2026-5465
Preprint. Discussion started: 22 September 2026


# Late Early Cretaceous Extension along the Southeastern Coast of China: Evidence from the Yunqicun Diorites, Northern Fujian

Hui. Su[1], Guishan. Zhang[1,2], Peng. Guo[1], Sen Lao[1], Yumeng Li[1]

[1]School of Earth Sciences and Resources, Chang'an University, Xian, 710000 , China
[2]Laboratory of Mineralization and Dynamics, Chang'an University, Xian, 710000, China

*Correspondence to*: Guishan. Zhang (zygszh@chd.edu.cn)

**Abstract.** The timing and geodynamic implications of late Early Cretaceous extension along the southeastern continental margin of China remain debated. To better constrain this issue, we investigate the Yunqicun diorites from northern Fujian using geochronological, geochemical, isotopic, and mineralogical approaches. Zircon U-Pb dating yield an emplacement age of 114.3 ± 2.1 Ma. The Yunqicun diorites exhibit isotopically enriched source signature, reflected by the elevated $(^{87}Sr/^{86}Sr)_i$ ratios (0.7119–0.7122) and negative $\varepsilon_{Nd}(t)$ values (-8.7 to -8.4). Their high La/Nb (3.35 – 4.28), Th/Ta (17.41 – 18.94), and La/Ta (53.47 – 66.67) ratios suggest modification of the mantle source by subduction-related components. Geochemical mixing trends and Sr-Nd isotopic modeling indicate involvement of ancient crustal components during subsequent magma evolution. The Yunqicun magmas underwent substantial fractional crystallization of plagioclase, amphibole, biotite, and clinopyroxene, as evidenced by low $Mg^{\#}$ values (40.09 – 40.61), depleted Cr (14.1 – 20.3 ppm) and Ni (6.37 – 7.60 ppm) contents, negative Eu anomalies, and whole-rock geochemical trends. Mineral thermobarometric calculations further constrain the crystallization history, revealing polybaric crystallization from deeper levels (~8 – 13 km) recorded by clinopyroxene to shallower levels (~1–3.5 km) indicated by amphibole and biotite. Zircon and hydrous minerals indicate that the Yunqicun magmas evolved under relatively oxidizing and water-rich conditions. Regional magmatic activity and crustal-thickness variations support coastal extension during ca. 125 – 105 Ma and demonstrate its persistence in northern Fujian. This extension likely reflects lithospheric reworking associated with Paleo-Pacific plate subduction.

## 1 Introduction

Late Mesozoic tectonomagmatic evolution in Southeast China was closely linked to the Paleo-Pacific plate subduction beneath the continental margin. This convergent-margin setting triggered widespread intrusive and volcanic magmatism, accompanied by extensive crustal reworking (Xu et al., 1999; Wu et al., 2019; Zhou and Li, 2000; Wei et al., 2023; Han et al., 2025). Cretaceous igneous rocks distributed across the region thus preserve a record of episodic variations in magmatic activity, tectonic regime transitions, and crust-mantle interactions (Qiu et al., 2008; Li et al., 2014, 2021; Shu et al., 2021; Zhao et al., 2023).

https://doi.org/10.5194/egusphere-2026-5465
Preprint. Discussion started: 22 September 2026


The geodynamic framework of Cretaceous magmatism and deformation in Southeast China remains debated despite decades of investigation. Existing interpretations invoke a range of processes related to changes in Paleo-Pacific subduction geometry and regional deformation, including models of progressive slab steepening, an early flat-slab stage followed by slab break-off and rollback, and ridge subduction (Zhou and Li, 2000; Li and Li, 2007; Sun et al., 2010). Recently, more studies have emphasized the role of lithospheric structure and composition in controlling regional tectonomagmatic evolution (Zhao et al., 2023). By combining igneous geochemistry with high-resolution shear-wave velocity imaging, Zhang et al. (2023) inferred that lithospheric delamination may have contributed to the compositional characteristics of Cretaceous magmatism in the region. Using two-dimensional geodynamic numerical simulations, Zhou et al. (2025) further explored a coupled subduction-delamination scenario linking deep lithospheric processes to the distribution of magmatism and basin development. However, the relationship between Cretaceous tectonomagmatic evolution and the structure of the lithosphere remains unresolved (Sun et al., 2007; Li et al., 2018; Wang et al., 2020).

The Cretaceous tectonic history of Southeast China involved alternating transpressional and extensional regimes (Cui et al., 2013; Li et al., 2014, 2021; Lin et al., 2021; Zheng et al., 2025). Structural investigations identify NW-SE-directed transpression at ca. 117 – 108 Ma, expressed by ductile deformation along the coastal Changle-Nan'ao Fault Zone and reduced magmatic activity (Li et al., 2014, 2024). Nevertheless, extensional deformation has also been recognized along the southeastern China coast (Wei et al., 2023; Han et al., 2025; Zheng et al., 2025; Zhou et al., 2025). Based on geochemical, thermochronological, and crustal-scale evidence, Zheng et al. (2025) proposed a prolonged transpressional interval from ca. 120 to 105 Ma, with extension developing in the coastal sector by ca. 105 Ma. Han et al. (2025) identified renewed magmatic activity at ca. 115 Ma along coastal Fujian, suggesting that magmatic reactivation occurred earlier along the coast than in the interior. Alternatively, Wei et al. (2023) argued that magmatism during the ca. 130–105 Ma was largely restricted to the Changle-Nan'ao Belt and was associated with slab-window opening. Thus, the timing, spatial extent, and geodynamic mechanism of late Early Cretaceous extension remain debated.

Dioritic magmas commonly incorporate mantle- and crust-derived components, making them valuable records of magma generation and crust-mantle exchange (Annen et al., 2006; Li et al., 2012; Ye et al., 2024). We therefore investigate the Yunqicun diorites in northern Fujian using petrological approach. These datasets are used to constrain the crystallization age, source characteristics, and petrogenetic evolution of the Yunqicun diorites. Combined with regional geochronological and crustal-thickness records, our results provide new constraints on the timing and geodynamic implications of late Early Cretaceous extension along the southeastern China coast.

https://doi.org/10.5194/egusphere-2026-5465
Preprint. Discussion started: 22 September 2026


## 2 Regional tectonic and magmatic framework

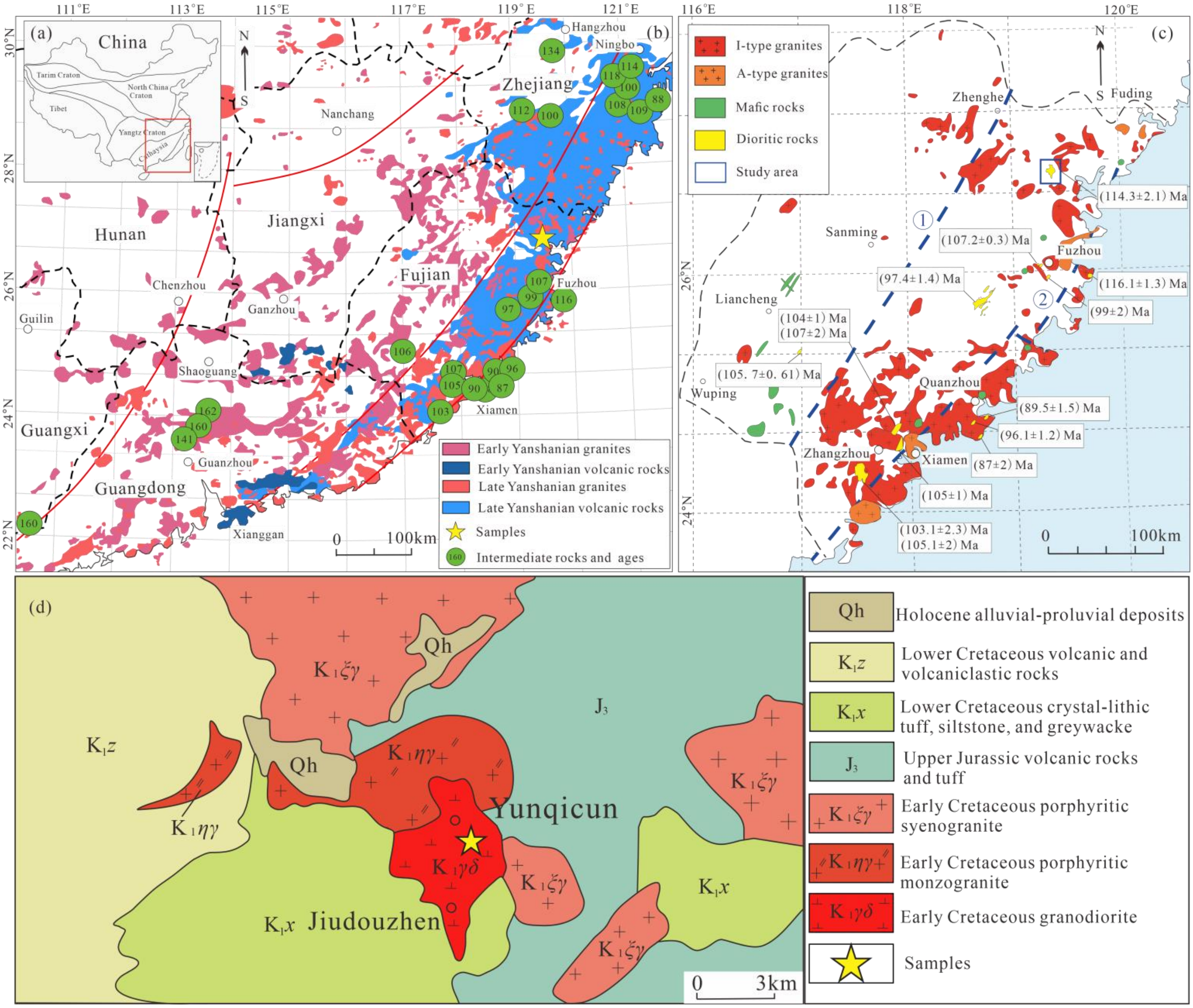


**Figure 1: (a) Simplified tectonic map of China (after Zheng et al., 2025); (b) Geological map showing the distribution of the Mesozoic magmatic rocks in Southeast China (after Zhou et al., 2006); (c) Geological map of the Cretaceous intrusive rocks in the Fujian Province, Southeast China (after Han et al., 2025 ); (d) Simplified geological map of the Yunqicun area and sample locations. ① Zhenghe-Dapu fault; ② Changle-Nan'ao fault. Data are in Table S1 in the Supplement.**

The South China Block is composed of the Yangtze and Cathaysia blocks, whose boundary is commonly delineated by the Jiangshan-Shaoxing and Pingxiang-Yushan faults (Zhao and Cawood, 2012)(Fig. 1a). Fujian occupies the eastern part of the Cathaysia Block and is divided into three major tectonic belts by the NNE-trending Zhenghe-Dapu and Changle-Nan'ao fault systems (Chen et al., 2002; Mao et al., 2014; Wang et al., 2017)(Fig. 1b). West of the Zhenghe-Dapu Fault lies the

Caledonian fold belt, which is characterized by Precambrian metamorphic basement rocks (Shen et al., 2018). Between the two fault zones, the Yanshanian magmatic belt contains abundant Cretaceous granitoids and rhyolites, with a pronounced south-north lithologic granitoid-rhyolite zonation (Zhao, 2004). Situated east of the Changle-Nan'ao Fault, the coastal belt mainly comprises regionally metamorphosed rocks, together with subordinate Late Mesozoic granitoids and mafic dykes (Chen et al., 2002; Wei et al., 2023).

In the eastern Cathaysia Block, particularly in Fujian and adjacent regions, Late Mesozoic magmatism exhibits a clear southeastward younging trend, as revealed by the spatial distribution of magmatic ages (Zhou and Li, 2000; Liu et al., 2020; Li et al., 2025)(Fig. 1b). Jurassic magmatism was dominated by granitic intrusions emplaced in the continental interior, whereas the Cretaceous magmatism involved widespread felsic to intermediate volcanic and plutonic rocks (Zhou et al., 2006; Li et al., 2016; Cao et al., 2021; Zheng et al., 2025). Cretaceous volcanic products are extensively exposed in Zhejiang and northeastern Fujian, consisting mainly of dacite, rhyolite, and tuff, with minor andesite (Guo et al., 2012). Coeval intrusive rocks are well developed in Fujian and dominated by granitic compositions, with lesser occurrences of granodiorite, quartz diorite, and gabbro (Xu et al., 1999) (Fig. 1c). Mafic to intermediate dykes represent another important component of the magmatic system and are commonly aligned with regional structural zones, indicating a close link between magma transport and tectonic structures (Wang et al., 2017, 2020; Lei et al., 2021). The close spatial association of gabbro-granite complexes provides evidence for interaction between mafic and felsic magmas in Fujian (Li et al., 2012, 2014, 2016) (Fig. 1c).

The Yunqicun dioritic intrusion is exposed in the Ningde area, northern Fujian (Fig. 1c), where it was emplaced into volcanic sequences of the Late Jurassic Nanyuan Formation and Early Cretaceous Xiaoxi Formation. The intrusion is locally covered by Quaternary deposits (Fig. 1d).

## 3 Petrographic characteristics

The Yunqicun diorites are gray to sage green and medium grained (Figs. 2a and b). Their mineral assemblage is mainly composed of plagioclase (55–60 %), biotite (10–15 %), and quartz (5–10 %), with amphibole and pyroxene occurring in smaller proportions. Apatite, magnetite, and zircon occur as accessory phases.

Plagioclase crystals are typically euhedral to subhedral and tabular, generally 0.3–1.1 mm in size (Figs. 2c – e). They commonly exhibit polysynthetic twins and zoning textures, whereas localized sericite alteration occurs along some grains (Fig. 2f). Biotite occurs as dark-brown flakes and shows moderate chloritization (Figs. 2c–e). Anhedral quartz fills interstitial spaces among the earlier-formed minerals (Figs. 2c, d and f). Amphibole appears as greenish, euhedral to subhedral crystals, that is strongly chloritized (Figs. 2c and d).

https://doi.org/10.5194/egusphere-2026-5465
Preprint. Discussion started: 22 September 2026


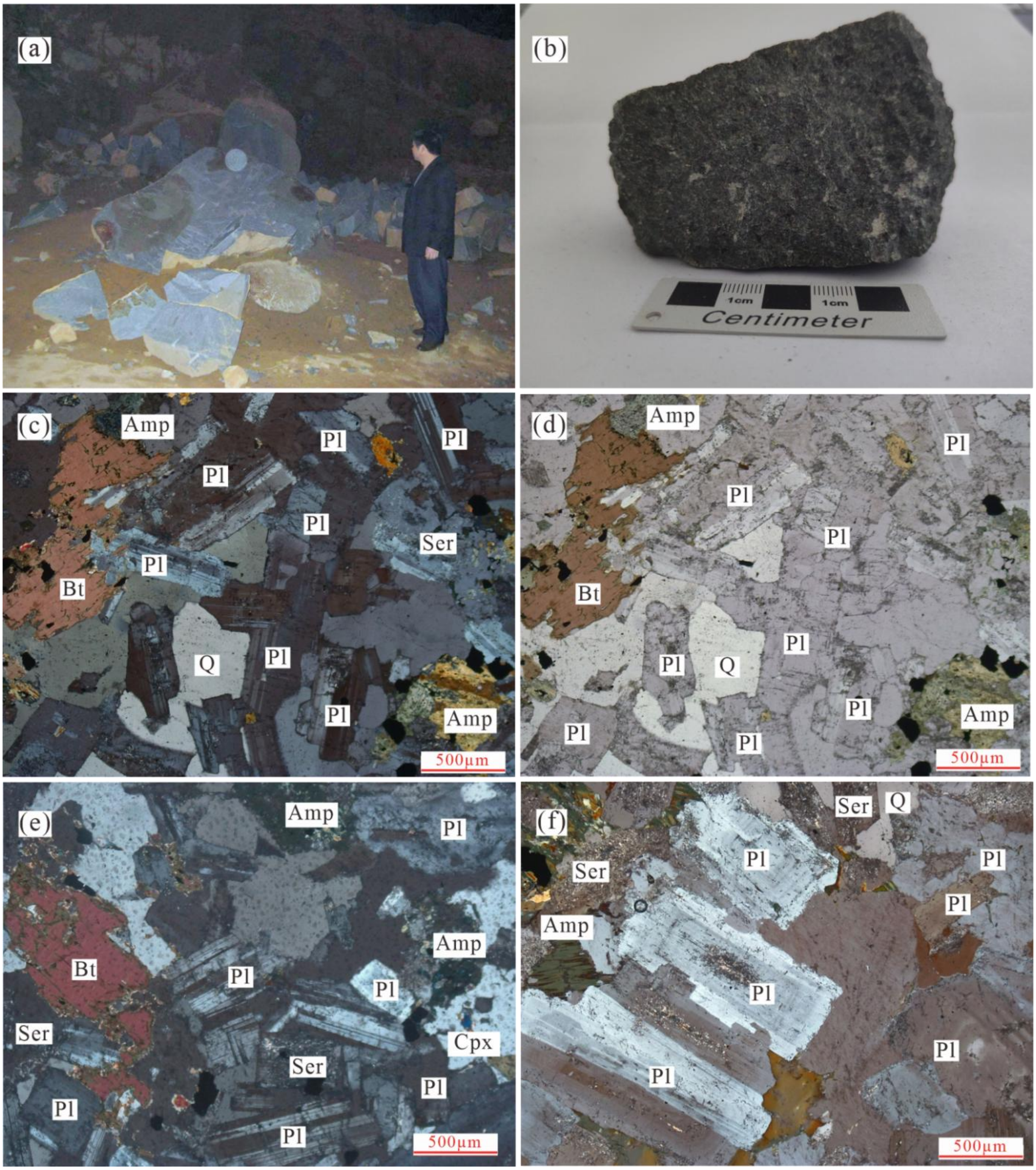


**Figure 2: Field and petrographic characteristics of the Yunqicun diorites. (a, b) Field outcrop of samples; (c, e) XPL and (d) PPL images illustrating the overall mineral assemblage; (f) XPL image showing zoning textures within plagioclase crystals. XPL-cross polarized light; PPL-plane polarized light. Pl-plagioclase; Bt-biotite; Amp-amphibole; Q-quartz; Cpx-clinopyroxene; Ser-sericite**

https://doi.org/10.5194/egusphere-2026-5465
Preprint. Discussion started: 22 September 2026


## 4 Analytical methods

We selected suitable zircon domains for analysis based on cathodoluminescence (CL) images before conducting U-Pb dating and trace-element measurements. Zircon domains were analyzed by LA-ICP-MS using a 193 nm ArF excimer laser system coupled with an Agilent 7500a ICP-MS at the State Key Laboratory of Continental Evolution and Early Life, Northwest University. We applied a 25 μm spot size during laser ablation. Zircon 91500 and NIST SRM 610 glass were used for U-Pb ages calibration and trace-element quantification, respectively. Analytical procedures followed the methods described by Yuan et al. (2004).

Whole-rock geochemical analyses were performed to determine major- and trace-element compositions. Major-element concentrations were obtained by X-ray fluorescence (XRF; LAB CENTER XRF-1800) at the Laboratory of Mineralization and Dynamics, Chang'an University, whereas trace-element concentrations were measured using an ELAN DRC-e ICP-MS at the State Key Laboratory of Critical Mineral Research and Exploration, Institute of Geochemistry, Chinese Academy of Sciences. The analytical precision was within 5 – 10% for major elements and <5% for trace elements. Further analytical details are provided by Qi et al. (2020).

We obtained Sr-Nd isotope data from whole-rock samples using the Nu Plasma 1700 MC-ICP-MS operated at the Guangzhou Institute of Geochemistry, Chinese Academy of Sciences. Instrumental mass fractionation was corrected by normalizing the measured Sr and Nd isotope ratios to $^{86}Sr/^{88}Sr=0.1194$ and $^{146}Nd/^{144}Nd = 0.7219$, respectively. Detailed analytical procedures are described in Liang et al. (2003).

Electron probe microanalysis (EPMA) using JXA-8100 provided mineral chemical compositions. The analyses were conducted at the Laboratory of Mineralization and Dynamics, Chang'an University. We performed the analyses under an accelerating voltage of 15 kV with beam currents of 10 or 20 nA. Peak and background counting times were set to 20 and 10 s, respectively, for Si, Mg, Fe, Al, Ca, Ti, and Mn, while Na and K were measured with counting times of 10 and 5 s.

## 5 Geochronological and geochemical results

The supplementary dataset includes zircon U-Pb ages (Table S2), whole-rock major- and trace-element compositions (Table S3), Sr-Nd isotope data (Table S4), and mineral chemical compositions (Table S5).

### 5.1 Zircon U-Pb ages and trace-element characteristics

Zircon grains from the Yunqicun diorites commonly display euhedral to subhedral forms, with transparent and colourless crystals ranging from 65 to 170 μm in length. Oscillatory zoning observed in CL images, together with Th/U ratios of 0.71–1.29, is consistent with a magmatic origin (Hoskin et al., 2003) (Fig. 3). A weighted mean $^{206}Pb/^{238}U$ age of 114.3±2.1 Ma (MSWD=2.7) was calculated from 19 zircon analyses (Fig. 4).

https://doi.org/10.5194/egusphere-2026-5465
Preprint. Discussion started: 22 September 2026


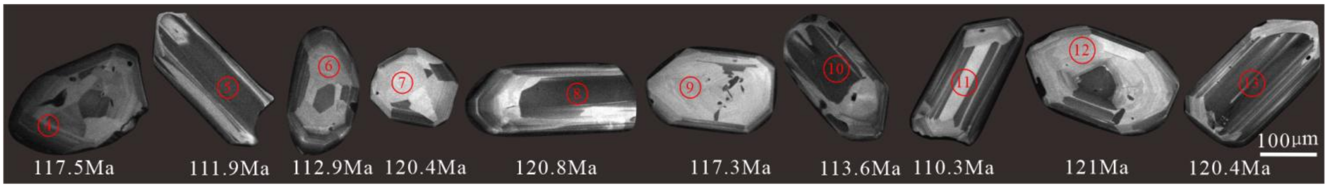


**Figure 3: Representative zircon CL images of the Yunqicun diorites. The red solid circles indicate the U-Pb dating sites**

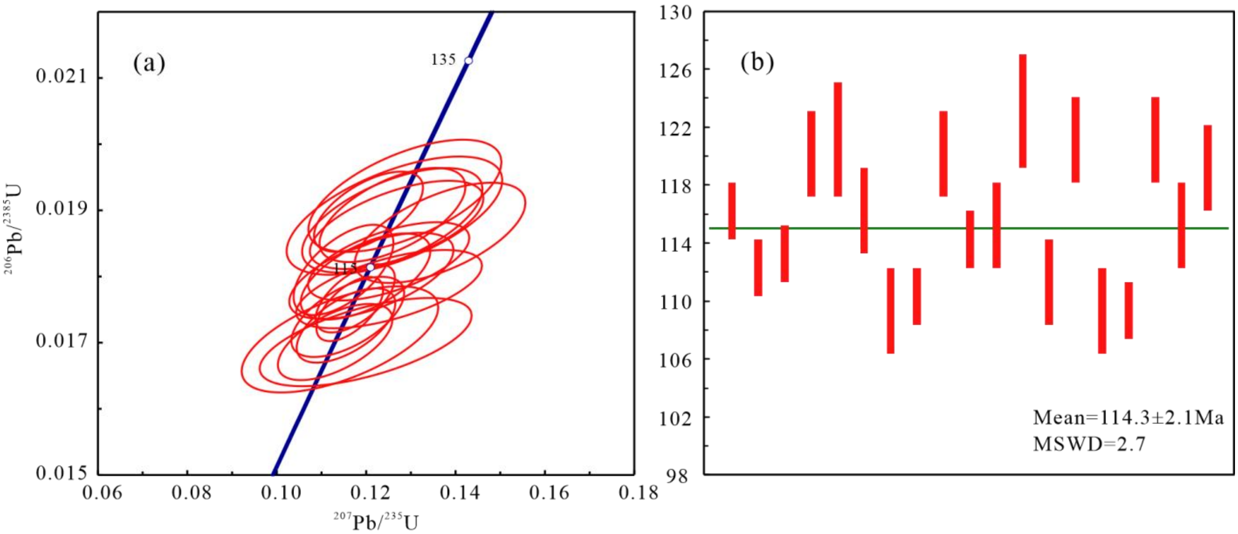


**Figure 4: Concordia diagrams for zircon LA-ICP-MS U-Pb analyses**

Zircons analyzed have ΣREE values of 321.90–1446.48 ppm (average 628.04 ppm), ΣLREE values of 15.65–72.51 ppm (average 28.75 ppm), ΣHREE values of 300.35–1400.81 ppm(average 599.29 ppm), LREE/HREE ratios of 0.03–0.15, δEu values of 0.15–0.26 (average 0.21), and δCe values of 1.88–192.78 (average 47.67). On chondrite-normalized REE patterns (Fig. S1 ), these spots exhibit depletion of LREEs, enrichment of HREEs, negative Eu anomalies, and positive Ce anomalies, which are characteristic of magmatic zircon.

### 5.2 Whole-rock geochemical characteristics

The Yunqicun diorites have $SiO_2$ and $Al_2O_3$ contents ranging from 60.75–61.34 wt.% and 15.79–16.04 wt.%. $Na_2O$ and $K_2O$ contents range from 3.75 to 3.88 wt.% and 2.97 to 3.22 wt.%, respectively. The samples plot in the diorite field on the TAS diagram (Fig. 5a) and display high-K calc-alkaline affinities (Figs. 5b and c). With A/CNK ratios of 0.87–0.90 and A/NK ratios of 1.75–1.88, all samples plot in the metaluminous field (Fig. 5d).

https://doi.org/10.5194/egusphere-2026-5465
Preprint. Discussion started: 22 September 2026


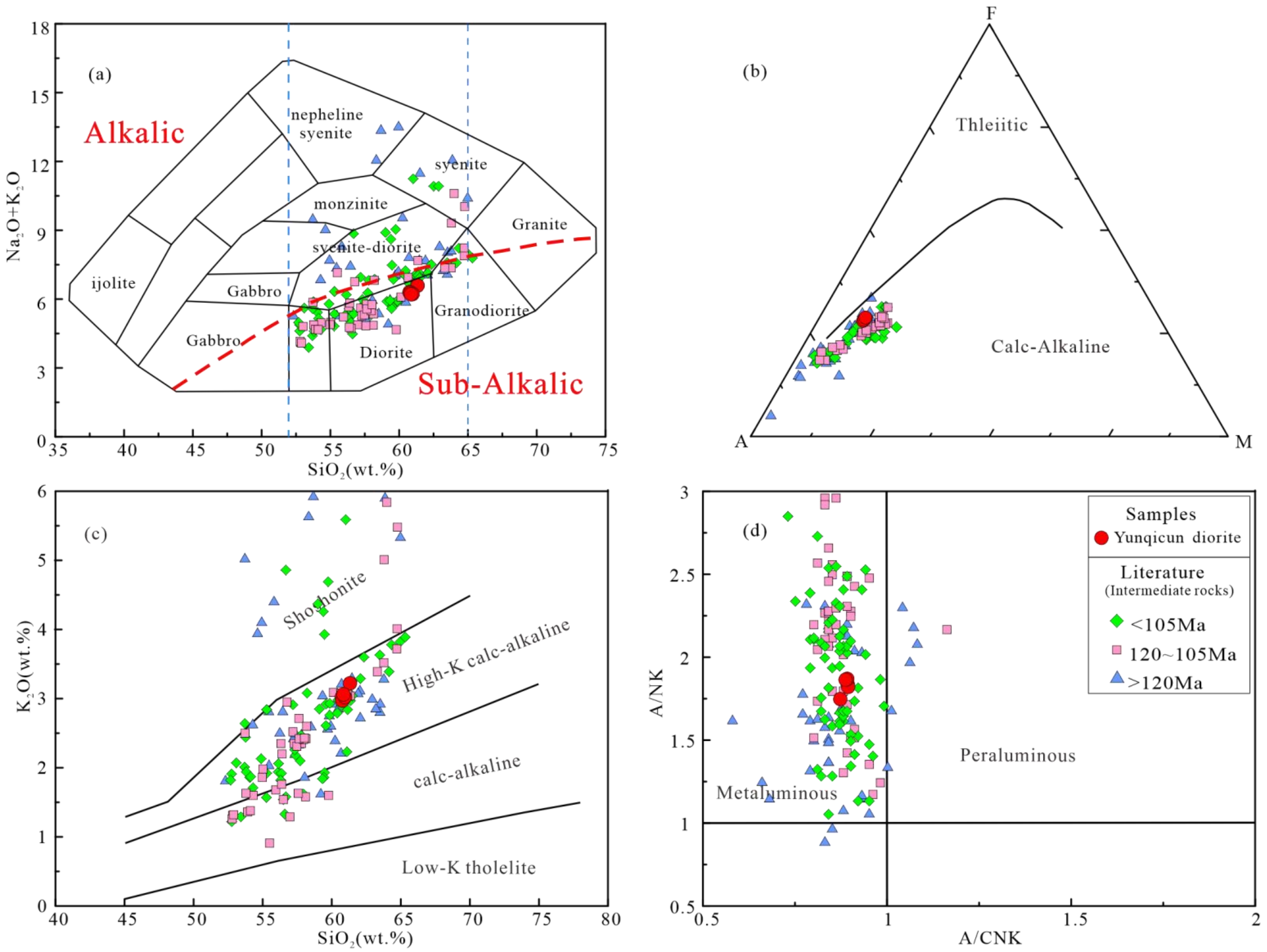


**Figure 5: Whole-rock geochemical classification of the Yunqicun diorites. (a) TAS diagram modified after Middlemost (1994). (b) AFM diagram modified after Irvine and Baragar (1971). (c) $K_2O$-$SiO_2$ diagram modified after Rickwood (1989). (d)A/CNK-A/NK diagram modified after Maniar and Piccoli (1989). Sources of comparative data are listed in Table S1.**

The Yunqicun diorites have ΣREE values ranging from 164.19–204.87 ppm. Their chondrite-normalized REE patterns show pronounced LREE-HREE fractionation and negative Eu anomalies (δEu=0.71–0.78), with $(La/Yb)_N$ ratios of 11.12–13.64 and LREE/HREE ratios of 9.11–10.96 (Fig. 6a). The samples are LILE enrichment (Rb, Ba, Pb, and K) and HFSE depletion (Nb, Ta, Ti, and Zr) (Fig. 6b).

https://doi.org/10.5194/egusphere-2026-5465
Preprint. Discussion started: 22 September 2026


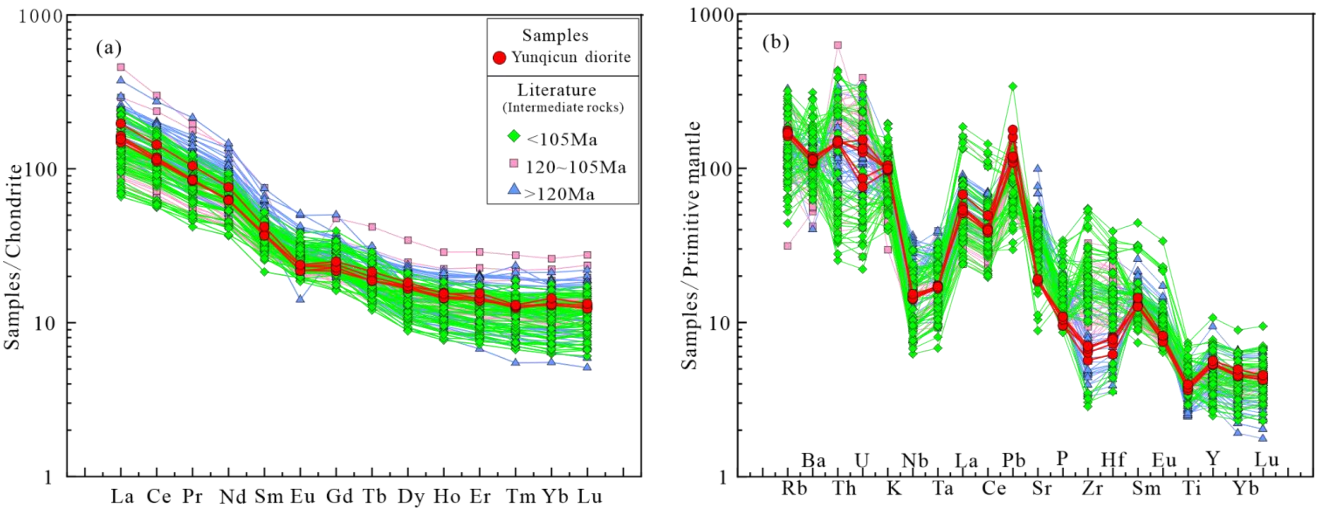


**Figure 6: Trace-element characteristics of the Yunqicun diorites. (a) Chondrite-normalized REE patterns. (b) primitive-mantle-normalized trace element patterns. Normalization values follow Sun and McDonough (1989). Sources of comparative data are listed in Table S1.**

### 5.3 Whole-rock Sr-Nd isotopic compositions

Figure 7 summarizes the Sr-Nd isotopic compositions of the Yunqicun diorites. Using the zircon U-Pb crystallization age, $(^{87}Sr/^{86}Sr)_i$ ratios and $\varepsilon_{Nd}(t)$ values were calculated to be 0.711927–0.712187 and -8.7 to -8.4, respectively. The corresponding $T_{DM2}$ ages are 1597–1620 Ma.

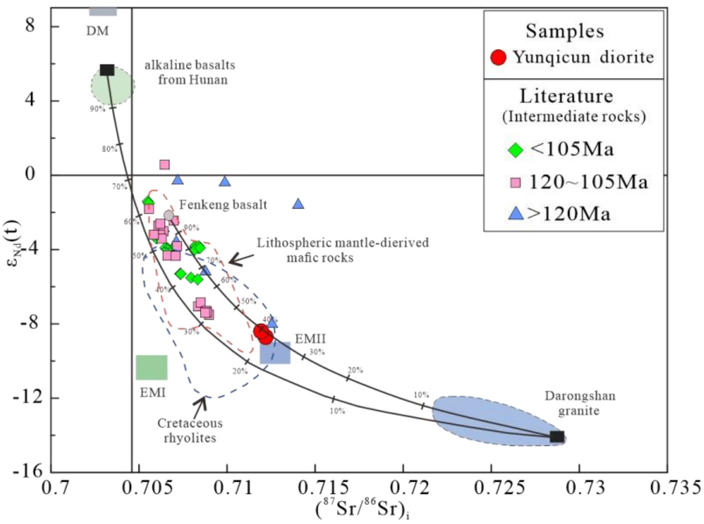


**Figure 7: Sr-Nd isotopic relationships of the Yunqicun diorites. Binary mixing curves were modeled using Fenkeng basalt (Chen et al., 2008) and Darongshan granite (Hsieh et al., 2008) as representative mantle-derived and silicic components, respectively, with alkaline basalts from Hunan included as an additional mantle reference (Li et al., 2004). Cretaceous Lithospheric mantle-dierived mafic rocks and rhyolites reported by Chen et al (2008) and Meng et al (2012) are shown for comparison. Tick marks represent 10% mixing increments. Sources of comparative data are listed in Table S1.**

https://doi.org/10.5194/egusphere-2026-5465
Preprint. Discussion started: 22 September 2026


## 5.4 Mineral chemical compositions

The analyzed biotite grains have FeO, $TiO_2$ and $Al_2O_3$ contents ranging from 17.32–19.89 wt.%, 3.68–4.47 wt.% and 12.19–13.19 wt.%, respectively, with $Mg^{\#}$ values of 0.49–0.56. Structural formulae calculated on the basis of 11 oxygen atoms indicat that K, Mg, Fe, and Al are the principal cations (K:0.75–0.93 apfu; Mg:1.22–1.48 apfu; $Fe^{2+}$:0.8–1.09 apfu; $Al^{IV}$:1.07–1.21 apfu). The biotite compositions indicate an Mg-rich character and correspond to the field of primary magmatic biotite on the $10\times TiO_2$-FeO-MgO (Fig. 8a).

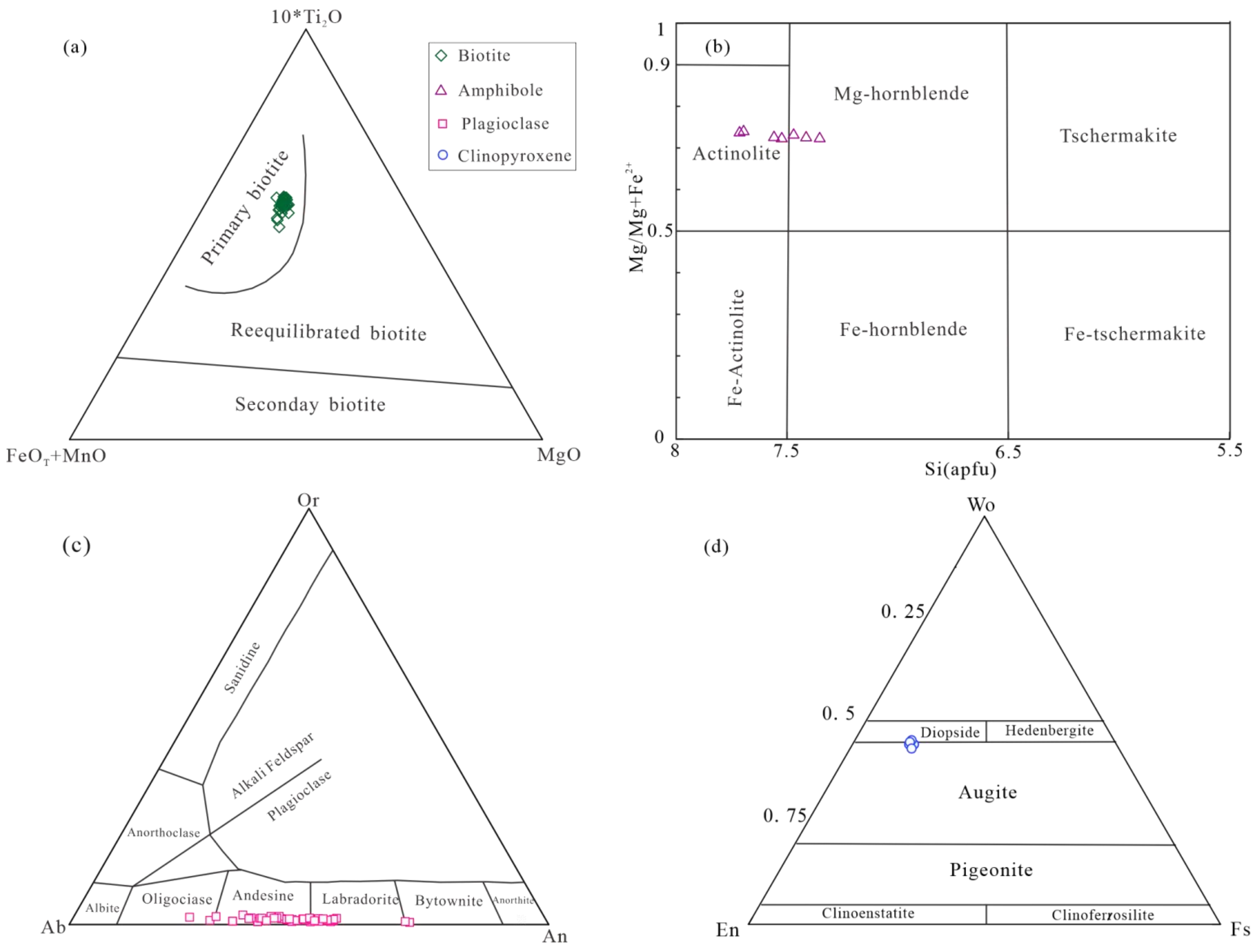


**Figure 8: Mineral chemical classification of the Yunqicun diorites. (a) biotite discrimination diagram modified after Nachit (2005). (b) amphibole classification diagram modified after Leake et al (1997). (c) feldspar Classification diagram modified after Deer et al (1992). (d) clinopyroxene classification diagram modified after Morimoto et al (1988).**

https://doi.org/10.5194/egusphere-2026-5465
Preprint. Discussion started: 22 September 2026


The analyzed amphibole grains show high MgO (14.22–15.09 wt.%) and CaO (11.47–11.88 wt.%) contents, whereas $K_2O$ (0.17–0.36 wt.%) and $Na_2O$ (0.41–0.86 wt.%) contents are relatively low. Based on the amphibole classification proposed by Leake et al. (1997), the $Na_B$ (0.12–0.21 apfu) and $Ca_B$ (1.79–1.85 apfu) values indicate that the analyzed grains belong to calcic amphibole group. The amphibole data points are distributed across the magnesiohornblende and actinolite domains in the classification diagram (Fig. 8b). The occurrence of actinolite compositions may reflect late-stage alteration or subsolidus re-equilibration.

The analyzed plagioclase grains have $SiO_2$ of 51.00–63.34 wt.%, $Al_2O_3$ of 23.61–31.62 wt.%, CaO of 4.85–14.26 wt.%, with $Na_2O$, $K_2O$, and FeO contents ranging from 3.25–8.24 wt%, 0.10–0.38 wt%, and 0.07–0.83 wt.%, respectively. Most plagioclase analyses plot within the andesine field of the Ab-Or-An diagram (Fig. 8c). Normal compositional zoning is common (e.g., YQ-4-13 and YQ-4-2), whereas reverse zoning occurs in a few grains (e.g., YQ-2-10).

The analyzed clinopyroxenes contain 14.41–14.92 wt.% MgO, 20.13–21.27 wt.% CaO, and 6.94–8.04 wt.% FeO. Cation proportions normalized to six oxygen atoms yield Ca=0.81–0.86, Mg=0.80–0.83, and $Fe^{2+}$=0.19–0.24 apfu. On the Wo-En-Fs ternary diagram, the analyses are classified as augite and diopside, with compositions of $Wo_{42.3\text{-}44.46}En_{42.29\text{-}43.29}Fs_{11.73\text{-}13.33}$ (Fig. 8d).

## 6 Discussion

### 6.1 Physicochemical conditions of magma crystallization

Magmatic evolution is controlled by a range of physicochemical parameters, including temperature, pressure, oxygen fugacity ($\log fO_2$), and melt $H_2O$ content. Mineral compositions preserve valuable records of these conditions and provide quantitative constraints on the crystallization history of igneous systems (Ferry and Watson, 2007; Putirka, 2008; Ridolfi et al., 2010).

The mineral thermometers provides temperature estimates spanning a wide interval, allowing reconstruction of the thermal evolution of the Yunqicun dioritic magma. The elevated temperatures obtained from plagioclase (1118.52–1182.65 ℃) and clinopyroxene (1054.22–1065.77 ℃) indicate that these minerals crystallized during the early high-temperature stage of magma evolution (Putirka, 2003, 2005) (Fig. 9a). In contrast, Ti-in-zircon thermometry yields lower temperatures of 752.6–839.90 ℃, with an average of 810.55 ℃. The dispersion of zircon temperatures likely reflects zircon crystallization over multiple stages during magma cooling and differentiation (Ferry and Watson, 2007) (Figs. 9a and 9b). Hydrous minerals yield the lowest temperature estimates, with biotite recording 711.77–743.95 ℃ (Henry et al., 2005) and amphibole 706.29–714.52 ℃ (Ridolfi et al., 2010) (Fig. 9a, c). Collectively, these mineral thermometers define a progressive cooling trajectory from early crystallization of plagioclase and clinopyroxene, through zircon growth during magma evolution, to late-stage amphibole and biotite crystallization.

https://doi.org/10.5194/egusphere-2026-5465
Preprint. Discussion started: 22 September 2026


The oxygen fugacity of the Yunqicun dioritic magma was estimated using mineral oxybarometers, with the calculated values summarized in Fig. 9a. Biotite-based oxybarometry based on Wones (1989) yields log$fO_2$ values ranging from -16.12 to -15.54. The position of biotite compositions above the NNO buffer in the $Fe^{2+}$-$Fe^{3+}$-Mg ternary diagram further indicates relatively oxidizing crystallization conditions (Fig. 9d). Amphibole oxybarometry proposed by Ridolfi et al. (2010) provides log$fO_2$ estimates of -14.25 to -14.04 (average -14.16), broadly consistent with the oxidizing conditions inferred from biotite oxybarometry (Fig. 9a). Zircon Ce-U-Ti oxybarometry further yields log$fO_2$ values of -14.38 to -12.77 (average -13.50) (Loucks et al., 2020). The consistent results obtained from multiple mineral oxybarometers suggests that the Yunqicun dioritic magma evolved under relatively oxidizing conditions throughout crystallization.

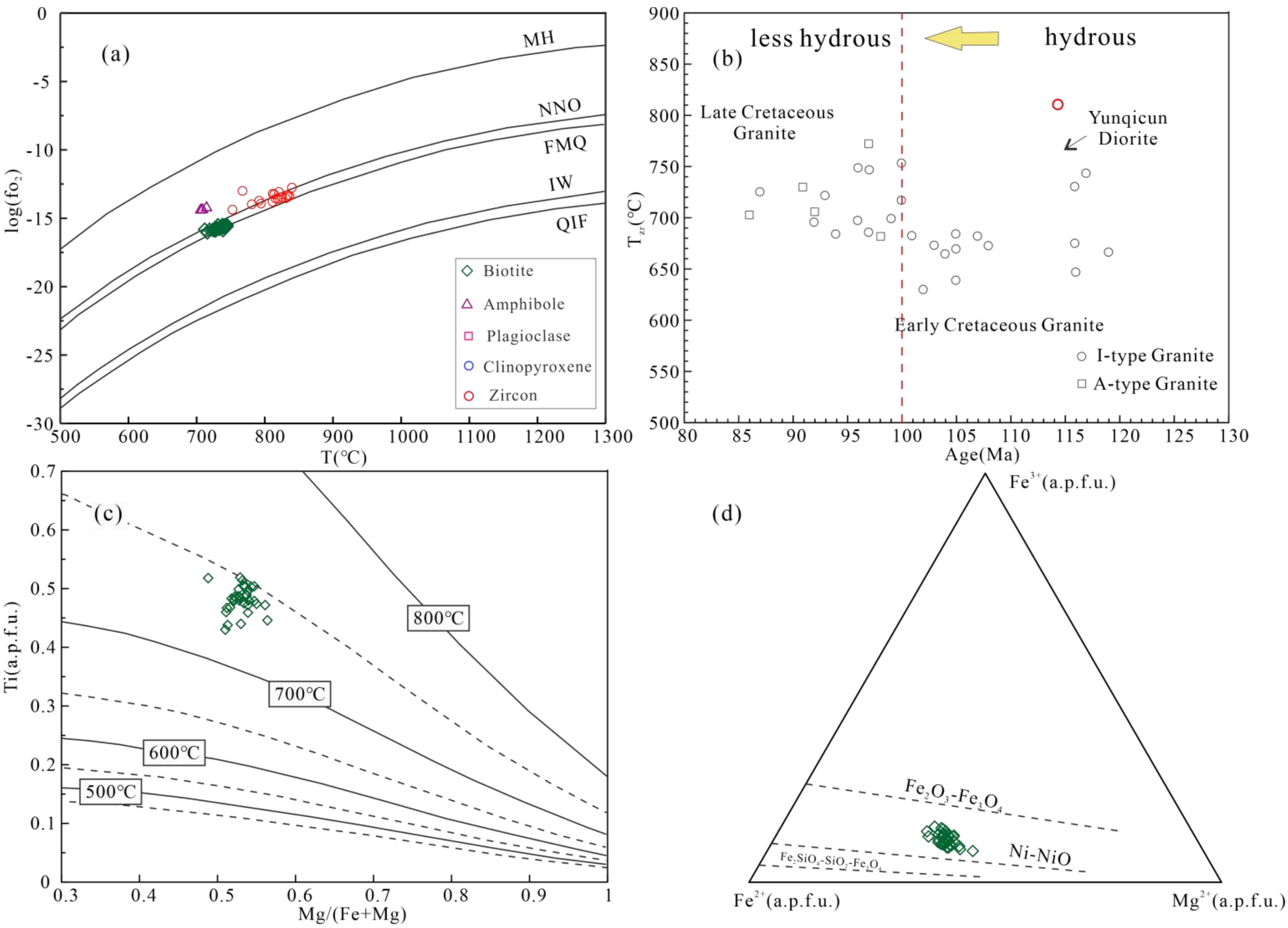


**Figure 9: (a) Relationship between lg($fO_2$) and T(°C) modified after Trail et al (2011). (b) Zircon saturation temperature versus Age diagram modified after Li et al (2018). (c) Biotite geothermometer diagram modified after Henry et al (2005). (d) Biotite compositions plotted on the $Fe^{3+}$-$Mg^{2+}$-$Fe^{2+}$ ternary diagram modified after Wones and Eugster (1965). NNO: nickel-nickel oxide buffer, FMQ: fayalite-magnetite-quartz buffer, HM: hematite-magnetite buffer, MW: magnetite-wustite buffer.**

Mineral-based pressure estimates reveal substantial variations in crystallization conditions within the Yunqicun dioritic magma system. Clinopyroxene-melt geobarometer following Putirka et al. (2003) gives pressure estimates of 2.22–3.42 kbar

https://doi.org/10.5194/egusphere-2026-5465
Preprint. Discussion started: 22 September 2026


(average 2.81 kbar), corresponding to storage depths of approximately 8.38–12.91 km (average 10.63 km). By comparison, amphibole barometry based on the calibration of Ridolfi et al. (2010) yields much lower pressures of 0.49–0.56 kbar, equivalent to depths of 1.85–2.11 km (average 1.99 km). Similarly, Al-in-biotite barometry following Uchida et al. (2007) indicates pressures of 0.29–0.92 kbar, corresponding to shallow depths of 1.08–3.49 km (average 1.85 km). The discrepancy between clinopyroxene-derived and hydrous mineral-derived pressures indicate that the Yunqicun magma dioritic system experienced crystallization across different crustal levels. Clinopyroxene likely records deeper magma storage, whereas amphibole and biotite represent shallower crystallization during subsequent magma evolution. This vertical pressure variation is consistent with magma ascent accompanied by cooling and continued crystallization.

The magmatic $H_2O$ contents during crystallization of the Yunqicun dioritic magma were estimated using zircon- and plagioclase-based hygrometers. The zircon hygrometer adapted from Ge et al. (2023) yields magmatic $H_2O$ contents of 5.33–7.54 wt.% (average 6.05 wt.%), using the median whole-rock major-element composition to approximate melt composition for calculating NBO/T(K). On the $T_{zr}$(°C)-Age(Ma) diagram (Fig. 9b), the Yunqicun diorites plot within the Early Cretaceous hydrous domain defined by previous studies(Li et al., 2018; Chen et al., 2024). In comparison, the plagioclase-melt hygrometer of Putirka (2008) provide slower $H_2O$ estimates ranging from 0.62 to 5.71 wt.% (average 3.24 wt.%). The difference between zircon- and plagioclase-derived $H_2O$ estimates likely reflects changes in melt volatile content and the crystallization stages recorded by different minerals. Progressive ascent and decompression may have facilitated $H_2O$ saturation and volatile exsolution (Brugger and Hammer, 2010; Waters et al., 2015). The abundant biotite phenocrysts in the Yunqicun diorites provide additional mineralogical evidence for crystallization from a water-rich magma system (Ridolfi et al., 2010; Richards, 2011).

Mineralogical and thermobarometric evidence suggests that the Yunqicun dioritic magma underwent polybaric crystallization and progressive cooling under hydrous and relatively oxidizing conditions. Clinopyroxene and plagioclase preserve evidence for an early, high-temperature crystallization stage, whereas amphibole and biotite reflect later crystallization at shallower crustal levels. Zircon geochronology and thermometry further define the temporal and thermal evolution of the magmatic system. Broadly consistent oxidation-state estimates from zircon, amphibole, and biotite indicate that relatively high oxygen fugacity characterized the magma during crystallization, whereas hygrometric estimates point to an $H_2O$-rich melt and are consistent with volatile loss during ascent and decompression. Collectively, these observations support a multilevel magma plumbing system for the Yunqicun diorites rather than a single crustal reservoir

### 6.2 Petrogenesis

Intermediate magmas can result from partial melting of the mafic lower crust (Atherton and Petford, 1993), differentiation of mantle-derived mafic magmas (Sisson and Grove, 1993), or slab-related modification of mantle sources by melts and/or fluids (Rogers and Hawkesworth, 1989; Hirose, 1997).

https://doi.org/10.5194/egusphere-2026-5465
Preprint. Discussion started: 22 September 2026


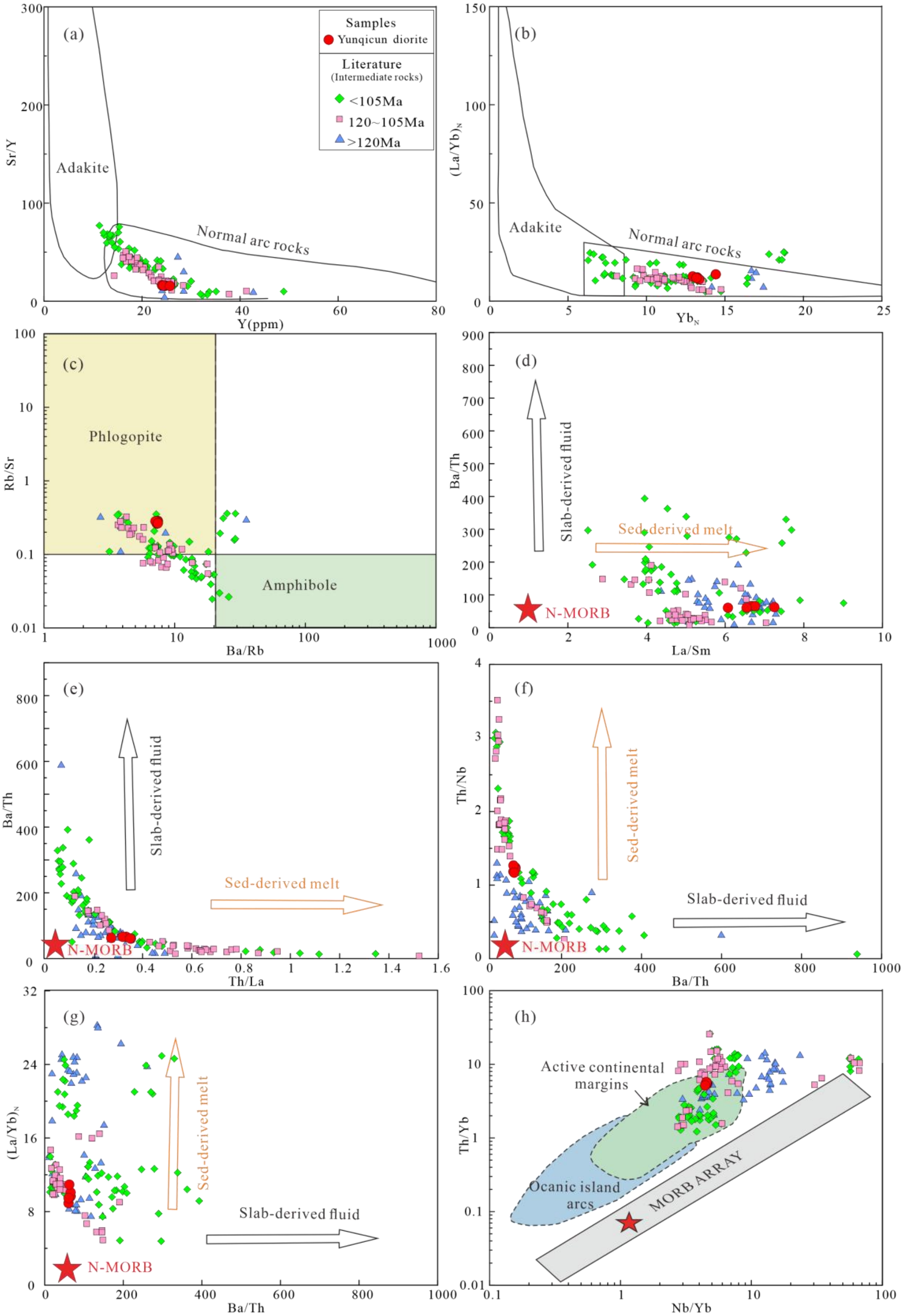

https://doi.org/10.5194/egusphere-2026-5465
Preprint. Discussion started: 22 September 2026


**Figure 10: (a, b) Sr/Y-Y and $Yb_N$-$(La/Yb)_N$ diagrams (after Defant and Drummond, 1990; Martin, 1999). (c) Rb/Sr versus Ba/Rb diagram modified after Furman and Graham (1999). (d-g) La/Sm-Ba/Th, Th/La-Ba/Th, Ba/Th-Th/Nb, and Ba/Th-$(La/Yb)_N$ diagrams. (h) Th/Yb versus Nb/Yb diagram modified after Pearce and Peate (1995). Sources of comparative data are listed in Table S1.**

Melts derived from crustal rocks typically exhibit low $Mg^{\#}$ values (<40), as demonstrated by dehydration melting experiments (Rapp and Watson, 1995), irrespective of the degree of melting (Rapp and Watson, 1995). By comparison, the Yunqicun diorites display slightly higher $Mg^{\#}$ values of 40.09–40.60. Their Nb/Ta ratios (14.42–15.59) also exceed the average value of lower crust (8.3; Rudnick et al., 2003). These features therefore are inconsistent with a model based solely on dehydration melting of lower-crustal rocks.

The Yunqicun diorites are characterized by low MgO (2.43–2.55 wt.%), Cr (14.13–20.3 ppm), and Ni (6.48–7.6 ppm) contents, which are differ from the geochemical signatures of high-Mg mantle-derived mafic magmas (Schmidt and Jagoutz, 2017; Zeng et al., 2021). Moreover, the lack of contemporaneous mafic rocks in the region provides little support for a simple mantle-derived fractional crystallization model.

The Yunqicun diorites display arc-like trace-element characteristics, including LREE enrichment relative to HREE, LILE enrichment, HFSE depletion, as well as high La/Nb (3.35–4.28), Th/Ta (17.41–18.94), and La/Ta (53.47–66.67) ratios (Hawkesworth et al., 1991). The samples plot within the field of normal arc rocks, further supporting subduction-related magmas (Figs. 10a and b). Sr-Nd isotopic compositions provide additional constraints on the magma source, with relatively high $(^{87}Sr/^{86}Sr)_i$ ratios (0.71219–0.71193) and low $\varepsilon_{Nd}(t)$ values (-8.7 to -8.4). The position of the samples in the Sr-Nd isotope diagram indicates involvement of an enriched lithospheric mantle component with an EMII-like signature (Fig. 7). Collectively, these constraints are best explained by a contribution from enriched lithospheric mantle that had previously been modified by subduction-derived materials.

The Yunqicun diorites display elevated Rb/Sr ratios (0.51–0.92) and low Ba/Rb ratios (1.05–2.57), corresponding to the phlogopite domain on the Rb/Sr-Ba/Rb diagram (Fig. 10c). This ratio pattern is consistent with a greater role for phlogopite than potassic amphibole in the mantle source, suggesting lithospheric mantle metasomatism by K-rich, volatile-bearing fluids or melts derived from subduction processes (Furman and Graham, 1999). The geochemical consequences of slab-derived fluids and sediment-derived melts differ during mantle metasomatism. Fluid-mobile elements such as Rb, Ba, K, Pb, and Sr are preferentially mobilized by aqueous fluids, whereas Th and LREEs are more readily supplied by sediment-derived melts (Hawkesworth et al., 1997; Furman and Graham, 1999; Pearce et al., 1999). The elemental relationships illustrated in Fig. 10d-g indicate modification of the lithospheric mantle by sediment-derived melts. The Yunqicun diorites show restricted Th/Yb ratios (5.18–5.76), and their position above the MORB-OIB array (Fig. 10h) are consistent with Th enrichment of the mantle source through the addition of sediment-derived melts. Together, these signatures record lithospheric mantle modification by sediment-derived melts during subduction.

https://doi.org/10.5194/egusphere-2026-5465
Preprint. Discussion started: 22 September 2026


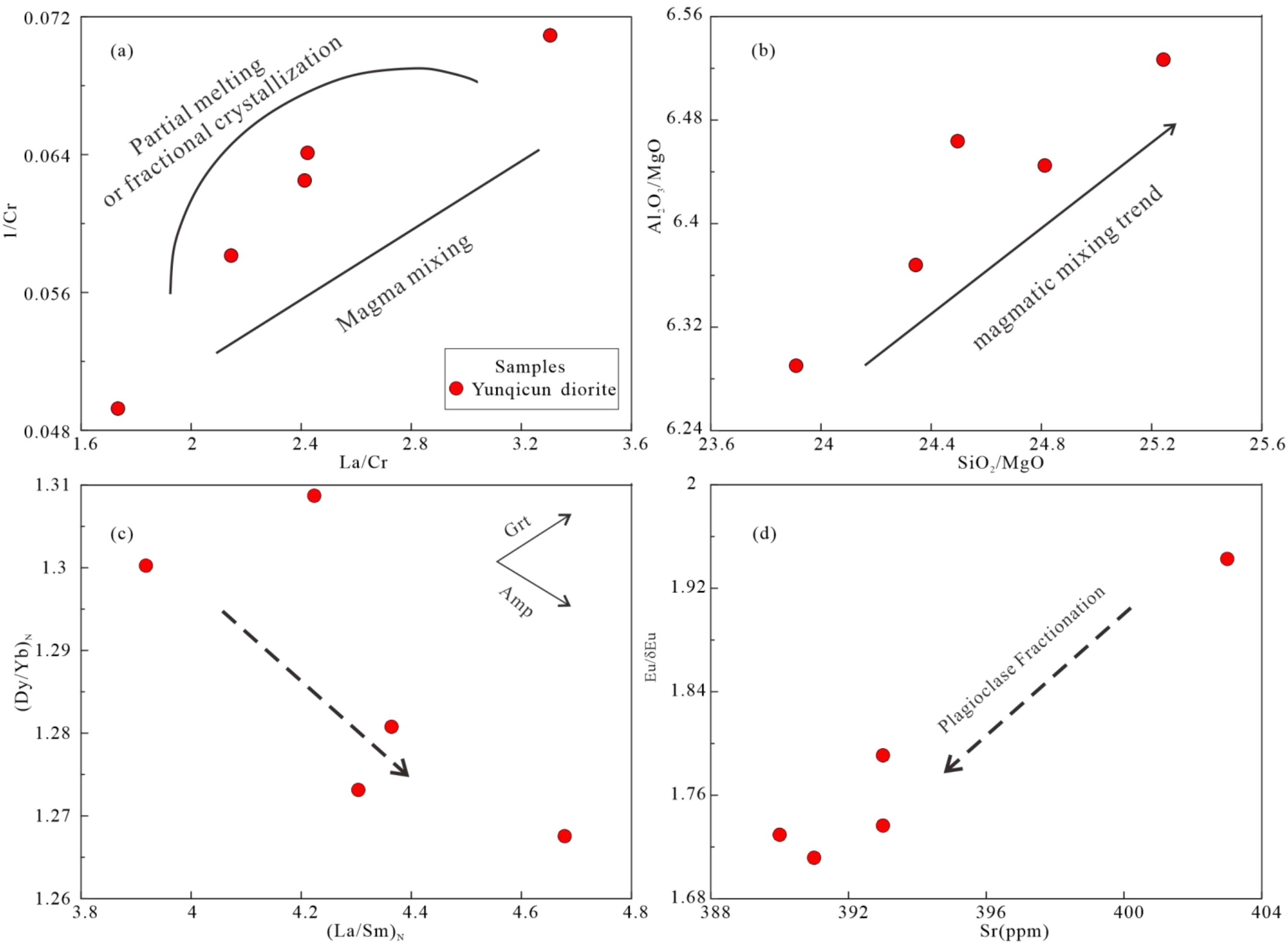


**Figure 11: (a) La/Cr-1/Cr diagram modified after Schiano et al (2010). (b) $SiO_2/MgO$-$Al_2O_3/MgO$ diagram modified after Tang et al (2021). (c) $(La/Sm)_N$-$(Dy/Yb)_N$ diagram. (d) Eu/δEu-Sr diagrams. Grt-garnet; Amp-amphibole.**

The compositional evolution of the Yunqicun magmas requires consideration of crustal inputs. The coherent trends displayed in Fig. 11a and b suggest mixing between compositionally distinct magma components. To evaluate this mixing process, a binary Sr-Nd isotopic mixing model was constructed using Fenkeng basalt (Li et al., 2004) and typical S-type granites (Hsieh et al., 2008) as mantle-derived and crustal end members, respectively. The calculated mixing trends reproduce the Sr-Nd isotopic compositions of the Yunqicun diorites, which overlap with those of coeval rhyolites, indicating contributions from both mantle-derived melts and recycled crustal materials (Fig. 7). Zircon Th/Y ratios calibrated by Turner et al. (2020) yield protolith $SiO_2$ contents of 57.09–64.06 wt.% (average 60.20 wt.%), placing the parental magmas of samples in the intermediate compositional range. These results hence support a magma evolution model involving mixing between mantle-derived and crustal components.

https://doi.org/10.5194/egusphere-2026-5465
Preprint. Discussion started: 22 September 2026


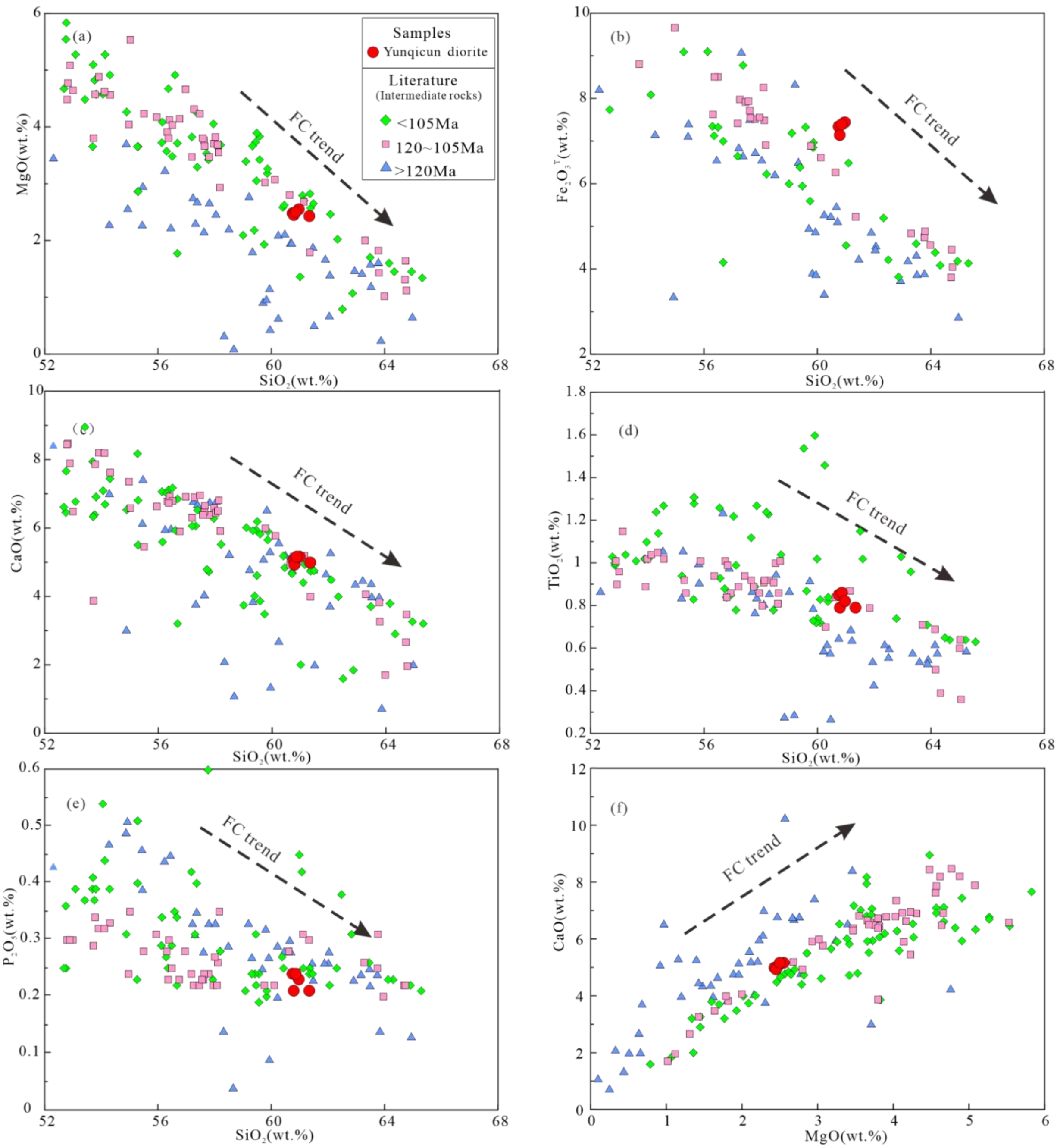


315 **Figure 12: (a-e)Harker diagram. (f) MgO-CaO diagram. Sources of comparative data are listed in Table S1.**

The Yunqicun diorites preserve evidence for substantial crystal fractionation during magma evolution. Compared with primitive mantle-derived magmas ($Mg^{\#}$:68–76, Cr:300–500 ppm, Ni:300–400 ppm), the Yunqicun diorites show lower $Mg^{\#}$ values (40.09–40.61) and depleted Cr (14.1–20.3 ppm) and Ni (6.37–7.6 ppm) contents, suggesting significant differentiation of the parental melts (Hess, 1992). The coupled decreases in MgO, $^{T}FeO$, and CaO with increasing $SiO_2$

https://doi.org/10.5194/egusphere-2026-5465
Preprint. Discussion started: 22 September 2026


reflect the progressive removal of Fe-Mg-Ca-bearing minerals, including clinopyroxene, amphibole, and biotite (Fig. 12a-c). The distribution pattern in the $(La/Sm)_N$-$(Dy/Yb)_N$ diagram highlights amphibole as an important fractionating phase (Fig. 11c), whereas the CaO-MgO covariation indicates significant clinopyroxene fractionation (Fig. 12f). Negative Eu, Ba, and Sr anomalies, combined with the Eu/δEu-Sr trend (Fig. 6 and 11d), suggest feldspar involvement, particularly plagioclase fractionation. The $TiO_2$-$SiO_2$ relationship (Fig. 12d) and Ti-Nb-Ta anomalies (Fig. 6b) point to rutile participation during differentiation. The negative correlation shown in Fig. 12e is consistent with apatite fractionation.

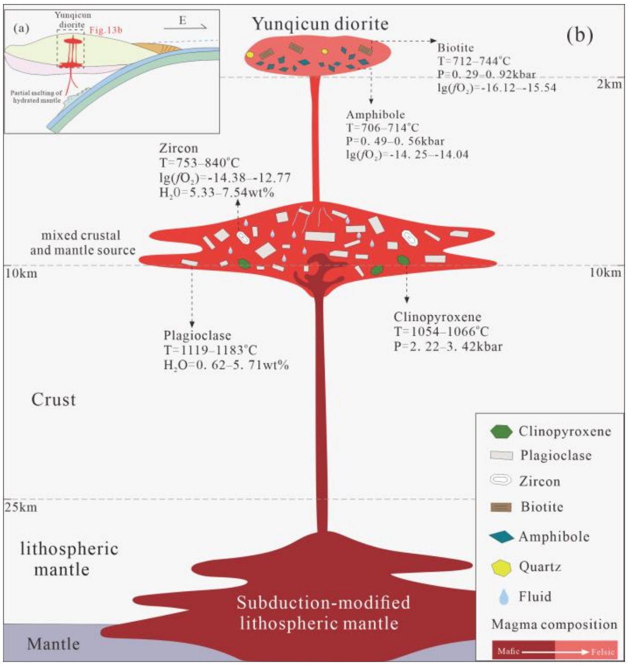


**Figure 13: Model for the petrogenesis of the Yunqicun diorites (modified from Wang et al., 2026). (a) Partial melting of the metasomatized asthenospheric mantle wedge generated primary magma of Yunqicun diorites; (b) Cartoons illustrating the preferred model of magma generation and evolution of the Yunqicun diorites**

The combined geochemical, isotopic, and mineral records outline a staged petrogenetic history for the Yunqicun diorites (Fig. 13). Melt generation began in lithospheric mantle that had inherited a subduction-related chemical imprint, with sediment-derived melts acting as an important metasomatic agent. During subsequent ascent through the crust, interaction with ancient crustal material further modified their compositions, as recorded Sr-Nd isotopic systematics and geochemical mixing trends. Crystallization was distributed across multiple crustal levels: clinopyroxene records deeper conditions at ~8–13 km, whereas amphibole and biotite crystallized later at shallower levels of ~1–3.5 km. Continued cooling promoted the progressive fractionation of plagioclase, amphibole, biotite, and clinopyroxene, ultimately producing the differentiated magmas emplaced in the shallow crust.

https://doi.org/10.5194/egusphere-2026-5465
Preprint. Discussion started: 22 September 2026


## 6.3 Tectonic implications

### 6.3.1 Cretaceous magmatic evolution and crustal thickness variations in Southeast China

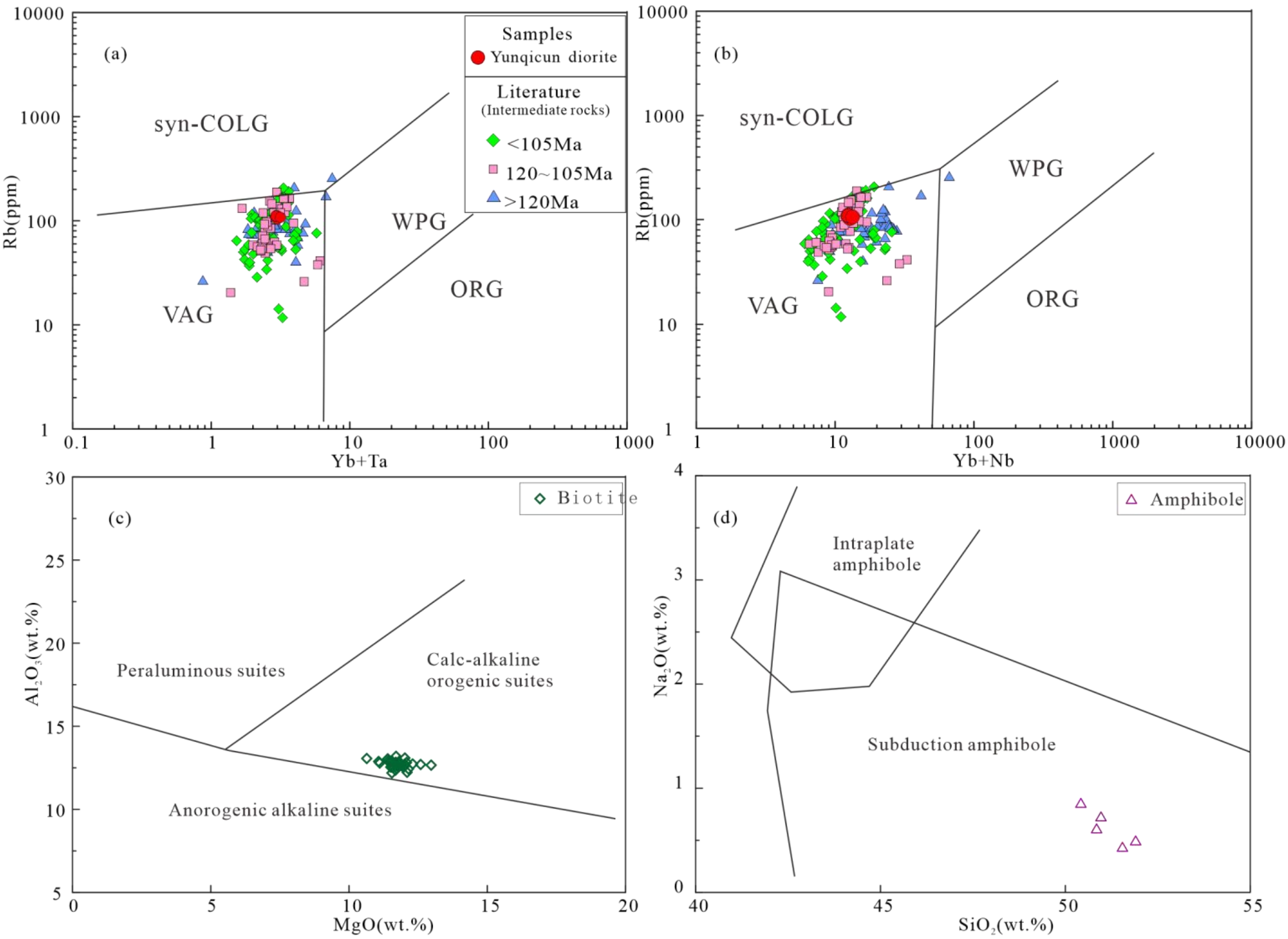


**Figure 14: Geochemical discrimination diagrams for tectonic setting. (a, b) Rb-Yb+Ta and Rb-Yb+Nb diagrams modified after Pearce et al (1984); (c) $Al_2O_3$-MgO diagram of biotite modified after Abdel-Rahman (1994); (d) $SiO_2$-$TiO_2$ diagram of amphibole modified after Coltorti et al (2007). VAG: volcanic arc granites; ORG: ocean ridge granites; WPG: within-plate granites; syn-COLG and post-COLG: syn-collisional and post-collisional granites. Published data sources are provided in Table S1.**

The Yb+Ta-Rb and Yb+Nb-Rb diagrams (Figs. 14a and b) place the Yunqicun diorites within the volcanic arc granite field, indicating an arc-related geochemical affinity. Biotite and amphibole compositions provide independent constraints on tectonic discrimination. In the MgO-$Al_2O_3$ diagram (Fig. 14c), biotite compositions correspond to the calc-alkaline orogenic field, a characteristic commonly associated with subduction-related magmatic systems. Amphibole compositions shown in Fig. 14d display a similar magmatic setting to that indicated inferred from biotite chemistry. Late Mesozoic magmatism in Southeast China is generally attributed to westward Paleo-Pacific Plate subduction and associated modification of the continental margin, which promoted crust-mantle interaction and magma generation (Zhou and Li, 2000; Li et al., 2024;

https://doi.org/10.5194/egusphere-2026-5465
Preprint. Discussion started: 22 September 2026


Zheng et al., 2025). Together, the Yunqicun diorites are interpreted as products of an active continental margin magmatic system.

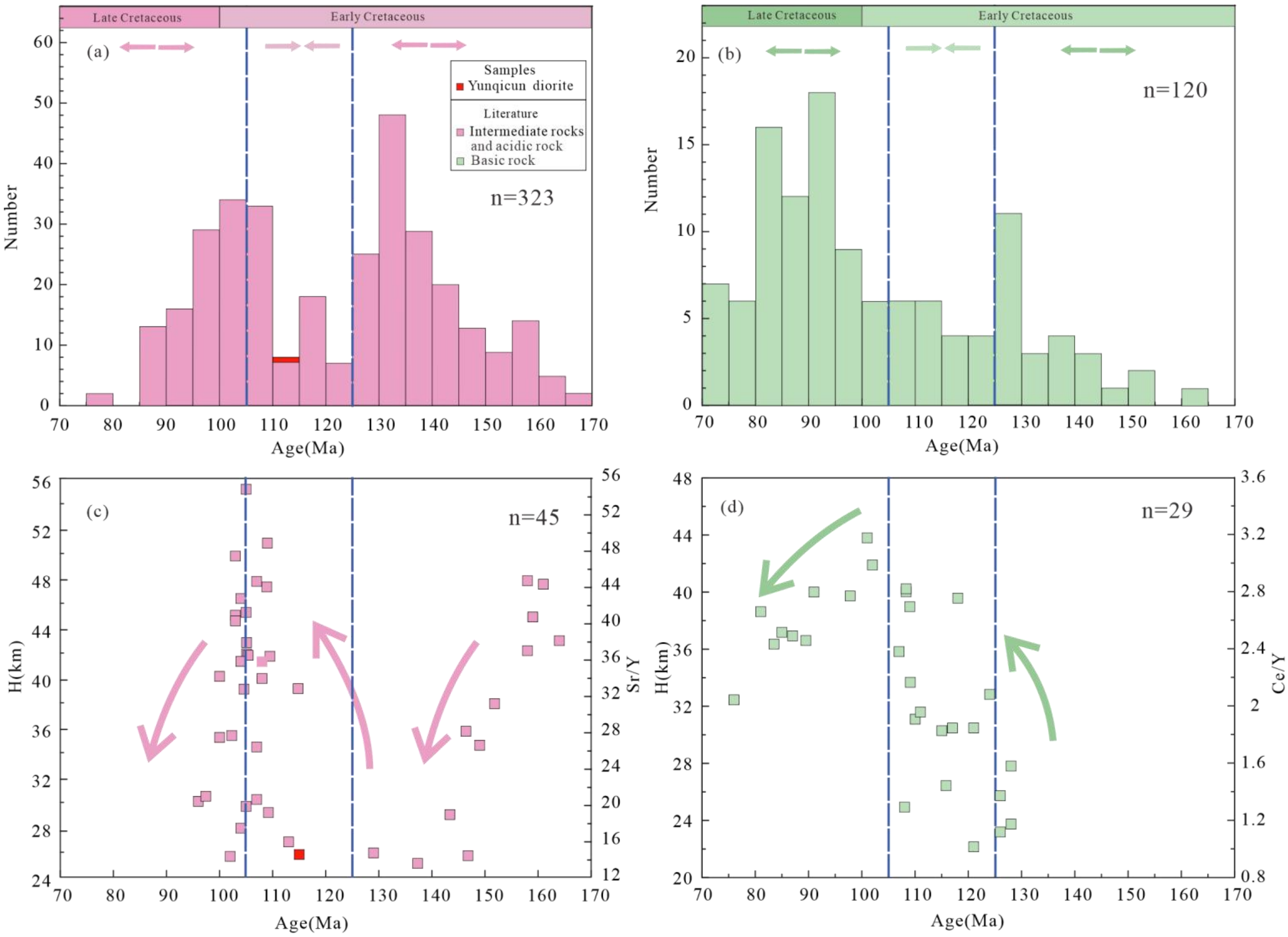


**Figure 15: Temporal evolution of Cretaceous magmatism and crustal thickness in Southeast China. (a, b) Kernel density estimate (KDE) distributions of zircon U-Pb ages. (c, d) crustal thickness-age relationships of Cretaceous magmatic rocks. Published data sources are provided in Tables S1 and S6.**

Published geochronological datasets define three distinct stages of Cretaceous magmatism in Southeast China (Fig.15a and b). During the early phase (145–125 Ma), felsic magmatism was dominant, represented mainly by A-type and I-type granitic intrusions (Table S1). Magmatic activity declined markedly between 125 and 105 Ma, representing a temporary lull in regional magmatism. Magmatic activity intensified again between 105 and 85 Ma, characterized by widespread I-type granitoids with increasing contributions from A-type granites and mafic rocks (Table S1). This temporal pattern records a transition from felsic-dominated magmatism in the Early Cretaceous, through a reduced magmatic interval, to increasingly diverse magmatism involving felsic and mafic components during the Late Cretaceous.

https://doi.org/10.5194/egusphere-2026-5465
Preprint. Discussion started: 22 September 2026


Reconstructed crustal thickness estimates reveal pronounced temporal variations in Southeast China during the Cretaceous (Fig. 15c and d). Crustal thickness evolution was reconstructed from published datasets comprising 199 Cretaceous magmatic samples, including 99 mafic, 39 intermediate, and 61 felsic rocks. Thickness estimates for intermediate to felsic and mafic samples were obtained using the Sr/Y calibration of Chapman et al. (2015) and the maximum Ce/Y approach of Mantle and Collins (2008), respectively. The reconstructed evolution show light crustal thinning from 145 to 125 Ma, followed by substantial thickening between 125 and 105 Ma, when the crust reached its maximum thickness of ~55.18 km. In contrast, the 114.3 Ma Yunqicun diorites were emplaced through relatively thin crust (~25.30 km), substantially thinner than crustal thickness estimates associated with most coeval magmatic rocks, suggesting pronounced spatial heterogeneity in crustal architecture. After 105 Ma, crustal thickness gradually declined to ~30–40 km between 105 and 85 Ma. This episodic crustal thickness evolution broadly parallels the temporal variation of Cretaceous magmatism in Southeast China, reflecting changes in crustal reworking and tectonic regime.

#### 6.3.2 Paleo-Pacific subduction-related Cretaceous tectonic evolution of Southeast China

The reconstructed geochronological framework documents a prolonged and episodic history of Cretaceous magmatism in Southeast China, highlighting temporal variations in magmatic activity and tectonic evolution. Based on compiled geochronological datasets and new results from this study, Cretaceous magmatism in Southeast China to be divided into three evolutionary stages (Fig. 16).

The 145–125 Ma interval is generally interpreted as a stage of Paleo-Pacific slab rollback, associated with widespread lithospheric extension across Southeast China (Chu et al., 2019; Li et al., 2014, 2021; Wei et al., 2023). This extensional setting promoted voluminous magmatism and the formation of NE-trending extensional basins, representing an active continental margin influenced by subduction processes (Zhou and Li, 2000; Qiu et al., 2022). Crustal thickness reconstruction indicates relatively thin crust during this interval (Fig. 16c and d). Intermediate rocks formed during this stage exhibit arc-like geochemical signatures, characterized by LREE and LILE enrichment, relative HREE and HFSE depletion, and pronounced Nb-Ta-Ti negative anomalies (Fig. 6a and b), reflecting derivation from a modified mantle source in a subduction-influenced setting (Pearce, 1983; Pearce and Peate, 1995; Zeng et al., 2025). Hence, these observations characterize an Early Cretaceous rollback-related extensional regime in Southeast China. Within this tectonic framework, subduction-related components likely modified the lithospheric mantle beneath Southeast China, generating a chemically enriched and fertile mantle source (Li et al., 2016, 2018). This metasomatized mantle source subsequently contributed to the parental magmas of the Yunqicun diorites (Fig. 16a).

During the second stage (125 – 105 Ma), Southeast China entered a transient transpressional regime characterized by diminished magmatic activity relative to the preceding extensional stage (Shu et al., 2009; Zhou and Li, 2000). Structural records from this interval include regional folding, Early Cretaceous strike-slip deformation, and sinistral ductile shearing along the coastal Changle-Nan'ao Fault (Shu et al., 2007; Li et al., 2014). Crustal thickness reconstruction further shows pronounced thickening between 125 and 105 Ma, when the crust reached a maximum thickness of ~55 km, consistent with

https://doi.org/10.5194/egusphere-2026-5465
Preprint. Discussion started: 22 September 2026


previous estimates (Fig. 15) (Li et al., 2024; Zheng et al., 2025). These lines of evidence suggest a transition from rollback-related extension to transpression during 125 – 105 Ma, possibly reflecting changes in regional plate interactions and convergence dynamics.

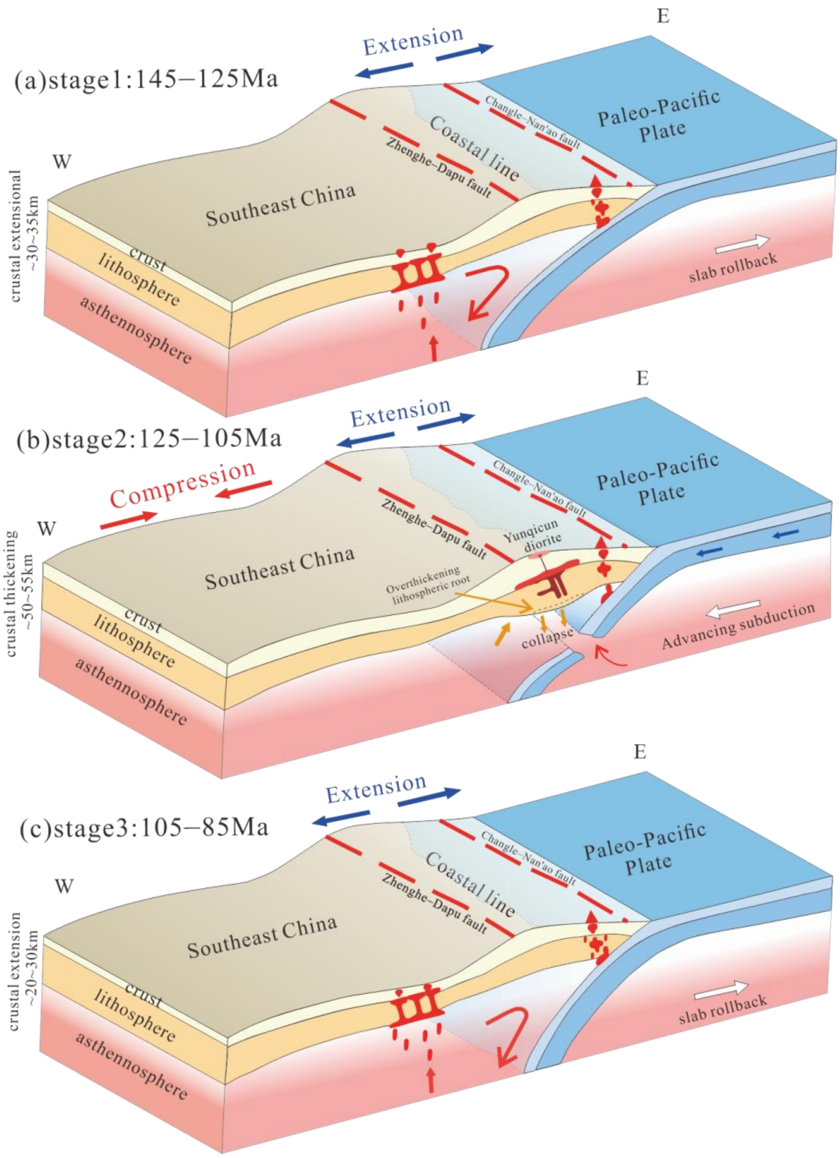


**Figure 16: Three-stage tectono-magmatic evolution model for the Yunqicun diorites and associated Cretaceous magmatism in Southeast China during Paleo-Pacific subduction.**

However, the regional response to this transpressional regime was not uniform. Inland areas underwent contractional deformation, as recorded by widespread angular unconformities, whereas coastal regions continued to experience extension, marked by the initiation of Upper Cretaceous sedimentation in coastal basins (Zheng et al., 2025). The persistence of coastal extension is further supported by the 115–90 Ma age peak of intrusive rocks in coastal Fujian Province (Li et al., 2019, 2023;

Han et al., 2025). The Yunqicun diorites, located within the coastal volcanic belt of Fujian Province, were emplaced through relatively thin crust (~25.30 km), contrasting with the thicker crust inferred for coeval magmatic rocks associated with regional compression (Fig. 16b). This feature is consistent with their formation in an extensional tectonic environment. Crustal thinning during 120–105 Ma has been attributed to processes such as lithospheric delamination (Zhou et al., 2025) and slab-window opening (Wei et al., 2022). The high temperatures, elevated $H_2O$ contents, and relatively oxidizing conditions of the Yunqicun magmas point to a role for water-fluxed melting during magma generation (Li et al., 2018). Such hydrous melt and/or fluid infiltration may have weakened the lithosphere and facilitated thinning, representing an additional process beyond delamination and slab-window mechanisms (Li et al., 2012, 2018).

During the 105–85 Ma interval, Southeast China returned to an extensional regime after the 125–105 Ma transpressional stage. The extensional regime was expressed by widespread A-type granitic magmatism, bimodal volcanism, and emplacement of mantle-derived mafic dykes, collectively defining an extensional tectono-magmatic system (Zhou and Li, 2000; Li et al., 2012; Li et al., 2015; Wang et al., 2017; Cai et al., 2023; Zhou et al., 2025). Extensional basins and widespread metamorphic core complexes provide additional structural evidence for regional extension (Shu et al., 2009). The transition from crustal thickening to thinning reflects a reorganization of the regional stress regime (Fig. 16c and d). Rather than representing an independent tectonic episode, the 105–85 Ma extension likely records the outward propagation of coastal extension that began during 125 – 105 Ma. Renewed rollback of the Paleo-Pacific slab likely supplied the geodynamic forcing responsible for this regional extension (Zhou and Li, 2020; Zheng et al., 2025).

## 7 Conclusions

1. Zircon U-Pb dating constrains the emplacement age of the Yunqicun diorites in northern Fujian to 114.3 ± 2.1 Ma (MSWD = 2.7), placing their emplacement within the late Early Cretaceous magmatic episode.

2. The Yunqicun diorites involved partial melting of a fertile lithospheric mantle source modified by Paleo-Pacific subduction, followed by crustal interaction and fractional crystallization involving plagioclase, amphibole, and biotite and clinopyroxene.

3. The Cretaceous tectono-magmatic evolution of Southeast China can be divided into three stages: early extension (145–125 Ma), a transitional transpressional stage with persistent coastal extension (125–105 Ma), and renewed widespread extension (105–85 Ma). The 125–105 Ma interval represents a spatially heterogeneous tectonic transition, characterized by regional transpression and continued extension in northern Fujian. This extensional component facilitated crustal thinning and contributed to the generation of the Yunqicun diorites, potentially involving lithospheric modification processes such as delamination, slab-window opening, and hydrous melt/fluid input.

Data availability. The supporting datasets are provided in the Supplement.

Author contributions. SH: conceptualization, methodology and preparation of the original draft. GZ: conceptualization, supervision, manuscript review and editing, and funding acquisition. GP: visualization. LS: data curation. LY: formal analysis.

Competing interests. The contact author has declared that none of the authors has any competing interests.

Financial support. This work was funded by the Key Project of Shaanxi Provincial Natural Science Foundation (grant no. 2025JC-QYXQ-013) and the National Natural Science Foundation of China (grant no. 41073027).

**References**

Abdel-Rahman, A. F. M.: Nature of biotites from alkaline, calc-alkaline, and peraluminous magmas, J. Petrol., 35, 525–541, https://doi.org/10.1093/petrology/35.2.525, 1994.

Annen, C., Blundy, J. D., and Sparks, R. S. J.: The genesis of intermediate and silicic magmas in deep crustal hot zones, J. Petrol., 47, 505–539, doi:10.1093/petrology/egi084, 2006.

Atherton, M. P. and Petford, N.: Generation of sodium-rich magmas from newly underplated basaltic crust, Nature, 362, 144–146, https://doi.org/10.1038/362144a0, 1993.

Brugger, C. R. and Hammer, J. E.: Crystallization kinetics in continuous decompression experiments: Implications for interpreting natural magma ascent processes, J. Petrol., 51, 1941–1965, https://doi.org/10.1093/petrology/egq044, 2010.

Cai, J. X., Wu, Y., and Han, Y. L.: Mafic to felsic dyke swarms in coastal Guangdong, China: Geochemical and geochronological constraints on the latest Mesozoic geodynamics on the southern margin of the South China Block, Geol. Mag., 160, 75–94, https://doi.org/10.1017/S0016756822000668, 2023.

Cao, X. Z., Flament, N., Li, S. Z., and Müller, R. D.: Spatio-temporal evolution and dynamic origin of Jurassic–Cretaceous magmatism in the South China Block, Earth-Sci. Rev., 217, 103605, https://doi.org/10.1016/j.earscirev.2021.103605, 2021.

Chapman, J. B., Ducea, M. N., DeCelles, P. G., and Profeta, L.: Tracking changes in crustal thickness during orogenic evolution with Sr/Y: An example from the North American Cordillera, Geology, 43, 919–922, https://doi.org/10.1130/G36996.1, 2015.

Chen, C. H., Lee, C. Y., and Shinjo, R.: Was there Jurassic paleo-Pacific subduction in South China?: Constraints from $^{40}Ar$-$^{39}Ar$ dating, elemental and Sr-Nd-Pb isotopic geochemistry of the Mesozoic basalts, Lithos, 106, 83–92, https://doi.org/10.1016/j. lithos.2008.06.009, 2008.

https://doi.org/10.5194/egusphere-2026-5465
Preprint. Discussion started: 22 September 2026


Chen, J. Y., Yang, J. H., Zhang, J. H., Zhu, Y. S., Sun, J. F., and Zhao, S. W.: Water content drives distinct evolution trajectory of Early Cretaceous granitoids in inland and coastal southeast China, Lithos, 488–489, 107836, https://doi.org/10.1016/j.lithos.2024.107836, 2024.

Chen, W. S., Yang, H. C., Wang, X., and Huang, H.: Tectonic setting and exhumation history of the Pingtan-Dongshan Metamorphic Belt along the coastal area, Fujian Province, Southeast China, J. Asian Earth Sci., 20, 829–840, https://doi.org/10.1016/S1367-9120(01)00066-9, 2002.

Chu, Y., Lin, W., Faure, M., Xue, Z. H., Ji, W. B., and Feng, Z. T.: Cretaceous episodic extension in the South China Block, East Asia: Evidence from the Yuechengling Massif of Central South China, Tectonics, 38, 3675–3702, https://doi.org/10.1029/2019TC005516, 2019.

Coltorti, M., Bonadiman, C., Faccini, B., Grégoire, M., O'Reilly, S. Y., and Powell, W.: Amphiboles from suprasubduction and intraplate lithospheric mantle, Lithos, 99, 68–84, https://doi.org/10.1016/j.lithos.2007.06.003, 2007.

Deer, W. A., Howie, R. A., and Zussman, J.: An Introduction to the Rock-Forming Minerals, 2nd edn., Longman Scientific & Technical, Harlow, 696 pp., 1992.

Defant, M. J. and Drummond, M. S.: Derivation of some modern arc magmas by melting of young subducted lithosphere, Nature, 347, 662–665, https://doi.org/10.1038/347662a0, 1990.

Ferry, J. M. and Watson, E. B.: New thermodynamic models and revised calibrations for the Ti-in-zircon and Zr-in-rutile thermometers, Contrib. Mineral. Petrol., 154, 429–437, https://doi.org/10.1007/s00410-007-0201-0, 2007.

Furman, T. and Graham, D.: Erosion of lithospheric mantle beneath the East African Rift system: Geochemical evidence from the Kivu volcanic province, Lithos, 48, 237–262, https://doi.org/10.1016/S0024-4937(99)00031-6, 1999.

Ge, R. F., Wilde, S. A., Zhu, W. B., and Wang, X. L.: Earth's early continental crust formed from wet and oxidizing arc magmas, Nature, 623, 334–339, https://doi.org/10.1038/s41586-023-06552-0, 2023.

Guo, F., Fan, W. M., Li, C. W., Zhao, L., Li, H. X., and Yang, J. H.: Multi-stage crust–mantle interaction in SE China: Temporal, thermal and compositional constraints from the Mesozoic felsic volcanic rocks in eastern Guangdong–Fujian provinces, Lithos, 150, 62–84, https://doi.org/10.1016/j.lithos.2011.12.009, 2012.

Han, Y., Li, X. Y., Yuan, X., Li, S. Z., Chen, X., Wang, P. C., Wang, Y., and Gao, J.: Petrogenesis and tectonic implications of Early Cretaceous I-type granites from offshore drilling in east of the Fuzhou City, Southeast China, Geosystems Geoenvironment, 4, 100400, https://doi.org/10.1016/j.geogeo.2025.100400, 2025.

Harris, N. B. W., Inger, S., and Xu, R. H.: Cretaceous plutonism in Central Tibet: An example of post-collision magmatism?, J. Volcanol. Geotherm. Res., 44, 21–32, https://doi.org/10.1016/0377-0273(90)90009-5, 1990.

Hawkesworth, C. J., Hergt, J. M., Ellam, R. M., and McDermott, F.: Element fluxes associated with subduction related magmatism, Philos. Trans. R. Soc. Lond. A, 335, 393–405, https://doi.org/10.1098/rsta.1991.0054, 1991.

Henry, D. J., Guidotti, C. V., and Thomson, J. A.: The Ti-saturation surface for low-to-medium pressure metapelitic biotites: Implications for geothermometry and Ti-substitution mechanisms, Am. Mineral., 90, 316–328, https://doi.org/10.2138/am.2005.1498, 2005.

https://doi.org/10.5194/egusphere-2026-5465
Preprint. Discussion started: 22 September 2026


Hess, P. C.: Phase equilibria constraints on the origin of ocean floor basalts, in: Mantle Flow and Melt Generation at Mid-Ocean Ridges, edited by: Phipps Morgan, J., Blackman, D. K., and Sinton, J. M., Geophys. Monogr. Ser., 71, 67–102, https://doi.org/10.1029/GM071p0067, 1992.

Hirose, K.: Melting experiments on lherzolite KLB-1 under hydrous conditions and generation of high-magnesian andesitic melts, Geology, 25, 42–44, https://doi.org/10.1130/0091-7613(1997)025%3C0042:MEOLKU%3E2.3.CO;2, 1997.

Hoskin, P. W. O. and Schaltegger, U.: The composition of zircon and igneous and metamorphic petrogenesis, Rev. Mineral. Geochem., 53, 27–62, https://doi.org/10.2113/0530027, 2003.

Hsieh, P. S., Chen, C. H., Yang, H. J., and Lee, C. Y.: Petrogenesis of the Nanling Mountains granites from South China: Constraints from systematic apatite geochemistry and whole-rock geochemical and Sr-Nd isotope compositions, J. Asian Earth Sci., 33, 428–451, https://doi.org/10.1016/j.jseaes.2008.02.002, 2008.

Irvine, T. N. and Baragar, W. R. A.: A guide to the chemical classification of the common volcanic rocks, Can. J. Earth Sci., 8, 523–548, https://doi.org/10.1139/e71-055, 1971.

Leake, B. E., Woolley, A. R., Arps, C. E. S., Birch, W. D., Gilbert, M. C., Grice, J. D., Hawthorne, F. C., Kato, A., Kisch, H. J., Krivovichev, V. G., Linthout, K., Laird, J., Mandarino, J. A., Maresch, W. V., Nickel, E. H., Rock, N. M. S., Schumacher, J. C., Smith, D. C., Stephenson, N. C. N., Ungaretti, L., Whittaker, E. J. W., and Guo, Y. Z.: Nomenclature of amphiboles: Report of the Subcommittee on Amphiboles of the International Mineralogical Association, Commission on New Minerals and Mineral Names, Am. Mineral., 35, 219–246, 1997.

Lei, Z. L., Zeng, G., Liu, J. Q., Wang, X. J., Chen, L. H., Zhang, X. Y., and Shi, J. H.: Melt-lithosphere interaction controlled compositional variations in mafic dikes from Fujian Province, southeastern China, J. Earth Sci., 32, 1445–1453, https://doi.org/10.1007/s12583-020-1358-y, 2021.

Li, B., Jiang, S. Y., Lu, A. H., Lai, J. Q., Zhao, K. D., and Yang, T.: Petrogenesis of Late Jurassic granodiorites from Gutian, Fujian Province, South China: Implications for multiple magma sources and origin of porphyry Cu–Mo mineralization, Lithos, 264, 540–554, https://doi.org/10.1016/j.lithos.2016.09.020, 2016.

Li, B., Jiang, S. Y., Lu, A. H., Zhao, H. X., Yang, T. L., and Hou, M. L.: Zircon U-Pb dating, geochemical and Sr–Nd–Hf isotopic characteristics of the Jintonghu monzonitic rocks in western Fujian Province, South China: Implication for Cretaceous crust–mantle interactions and lithospheric extension, Lithos, 260, 413 – 428, https://doi.org/10.1016/j. lithos, 2016.05.002, 2016.

Li, B., Jiang, S. Y., Zhang, Q., Zhao, H. X., and Zhao, K. D.: Cretaceous crust–mantle interaction and tectonic evolution of Cathaysia Block in South China: Evidence from pulsed mafic rocks and related magmatism, Tectonophysics, 661, 136–155, doi:10.1016/j.tecto.2015.08.032, 2015.

Li, C. L., Wang, Z. X., Lü, Q. T., Tan, Y. L., Li, L. L., and Tao, T.: Mesozoic tectonic evolution of the eastern South China Block: A review on the synthesis of the regional deformation and magmatism, Ore Geol. Rev., 131, 104028, https://doi.org/10.1016/j.oregeorev.2021.104028, 2021.

https://doi.org/10.5194/egusphere-2026-5465
Preprint. Discussion started: 22 September 2026


Li, H. Y., Chen, J. Q., Li, Z. B., Chen, X. F., Cai, H. T., Feng, X. P., Zhang, G. H., and Jin, Z.: Mid-crustal low-velocity zones beneath Southeastern Coastal China revealed by multimodal ambient noise tomography: Insights into Mesozoic magmatic activities, Tectonophysics, 898, 230636, https://doi.org/10.1016/j.tecto.2025.230636, 2025.

Li, J. H., Dong, S. W., Cawood, P. A., Thybo, H., Clift, P. D., Johnston, S. T., Zhao, G. C., and Zhang, Y. Q.: Cretaceous long-distance lithospheric extension and surface response in South China, Earth-Sci. Rev., 243, 104496, https://doi.org/10.1016/j.earscirev.2023.104496, 2023.

Li, J. H., Dong, S. W., Cawood, P. A., Zhao, G. C., Johnston, S. T., Zhang, Y. Q., and Xin, Y. J.: An Andean-type retro-arc foreland system beneath northwest South China revealed by SINOPROBE profiling, Earth Planet. Sci. Lett., 490, 170–179, https://doi.org/10.1016/j.epsl.2018.03.008, 2018.

Li, J. H., Zhang, Y. Q., Dong, S. W., and Johnston, S. T.: Cretaceous tectonic evolution of South China: A preliminary synthesis, Earth-Sci. Rev., 134, 98–136, https://doi.org/10.1016/j.earscirev.2014.03.008, 2014.

Li, S. Z., Suo, Y. H., Li, X. Y., Zhou, J., Santosh, M., Wang, P. C., Wang, G. Z., Guo, L. L., Yu, S. Y., Lan, H. Y., Dai, L. M., Zhou, Z. Z., Cao, X. Z., Zhu, J. J., Liu, B., Jiang, S. H., Wang, G., and Zhang, G. W.: Mesozoic tectono-magmatic response in the East Asian ocean-continent connection zone to subduction of the Paleo-Pacific Plate, Earth-Sci. Rev., 192, 91–137, https://doi.org/10.1016/j.earscirev.2019.03.003, 2019.

Li, X. H., Chung, S. L., Zhou, H. W., Lo, C. H., Liu, Y., and Chen, C. H.: Jurassic intraplate magmatism in southern Hunan–eastern Guangxi: $^{40}Ar/^{39}Ar$ dating, geochemistry, Sr-Nd isotopes and implications for the tectonic evolution of SE China, Geological Society, London, Special Publications, 226, 193–215, doi:10.1144/GSL.SP.2004.226.01.11, 2004.

Li, Z., Qiu, J. S., and Yang, X. M.: A review of the geochronology and geochemistry of Late Yanshanian (Cretaceous) plutons along the Fujian coastal area of southeastern China: Implications for magma evolution related to slab break-off and rollback in the Cretaceous, Earth-Sci. Rev., 128, 232–248, https://doi.org/10.1016/j.earscirev.2013.09.007, 2014.

Li, Z., Qiu, J. S., and Xu, X. S.: Geochronological, geochemical and Sr–Nd–Hf isotopic constraints on petrogenesis of Late Mesozoic gabbro–granite complexes on the southeast coast of Fujian, South China: Insights into a depleted mantle source region and crust-mantle interactions, Geol. Mag., 149, 459–482, doi:10.1017/S0016756811000793, 2012.

Li, Z., Wang, X. C., Wilde, S. A., Liu, L., Li, W. X., and Yang, X. M.: Role of deep-Earth water cycling in the growth and evolution of continental crust: Constraints from Cretaceous magmatism in southeast China, Lithos, 302-303, 126 – 141, https://doi.org/10.1016/j.lithos.2017.12.028, 2018.

Li, Z. X. and Li, X. H.: Formation of the 1300-km-wide intracontinental orogen and postorogenic magmatic province in Mesozoic South China: A flat-slab subduction model, Geology, 35, 179–182, https://doi.org/10.1130/G23193A.1, 2007.

Liang, X. R., Wei, G. J., Li, X. H., and Liu, Y.: Precise measurement of $^{143}Nd/^{144}Nd$ and Sm/Nd ratios using a multi-collector inductively coupled plasma mass spectrometer (MC-ICP-MS), Geochimica, 32, 91–96, 2003.

Lin, W., Zeng, J. P., Meng, L. T., Qiu, H. B., Wei, W., Ren, Z. H., Chu, Y., Li, S. J., Song, C., and Wang, Q. C.: Extensional tectonics and North China Craton destruction: Insights from the magnetic susceptibility anisotropy (AMS) of granite and metamorphic core complex, Sci. China Earth Sci. , 64, 1557–1589, https://doi.org/10.1007/s11430-020-9754-1, 2021.

https://doi.org/10.5194/egusphere-2026-5465
Preprint. Discussion started: 22 September 2026


Liu, J. X., Wang, S., Wang, X. L., Du, D. H., Xing, G. F., Fu, J. M., Chen, X., and Sun, Z. M.: Refining the spatio-temporal distributions of Mesozoic granitoids and volcanic rocks in SE China, J. Asian Earth Sci., 201, 104503, https://doi.org/10.1016/j.jseaes.2020.104503, 2020.

Loucks, R. R., Fiorentini, M. L., and Henríquez, G. J.: New magmatic oxybarometer using trace elements in zircon, J. Petrol., 61, egaa034, https://doi.org/10.1093/petrology/egaa034, 2020.

Maniar, P. D. and Piccoli, P. M.: Tectonic discrimination of granitoids, Geol. Soc. Am. Bull., 101, 635 – 643, https://doi.org/10.1130/0016-7606(1989)101%3C0635:TDOG%3E2.3.CO;2, 1989.

Mantle, G. W. and Collins, W. J.: Quantifying crustal thickness variations in evolving orogens: Correlation between arc basalt composition and Moho depth, Geology, 36, 87–90, https://doi.org/10.1130/G24095A.1, 2008.

Mao, J. R., Li, Z. L., and Ye, H. M.: Mesozoic tectono-magmatic activities in South China: Retrospect and prospect, Sci. China Earth Sci., 57, 2853–2877, https://doi.org/10.1007/s11430-014-5006-1, 2014.

Martin, H.: The adakitic magmas: Modern analogues of Archaean granitoids, Lithos, 46, 411 – 429, https://doi.org/10.1016/S0024-4937(98)00076-0, 1999.

Meng, L. F., Li, Z. X., Chen, H. L., Li, X. H., and Wang, X. C.: Geochronological and geochemical results from Mesozoic basalts in southern South China Block support the flat-slab subduction model, Lithos, 132 – 133, 127 – 140, https://doi.org/10.1016/j.lithos.2011.11.023, 2012.

Middlemost, E. A. K.: Naming materials in the magma/igneous rock system, Earth-Sci. Rev., 37, 215 – 224, https://doi.org/10.1016/0012-8252(94)90029-9, 1994.

Morimoto, N., Fabries, J., Ferguson, A. K., Ginzburg, I. V., Ross, M., Seifert, F. A., Zussman, J., Aoki, K., and Gottardi, G.: Nomenclature of pyroxenes, Am. Mineral., 73, 1123–1133, 1988.

Nachit, H., Ibhi, A., Abia, E. H., and Ben Ohoud, M.: Discrimination between primary magmatic biotites, reequilibrated biotites and neoformed biotites, C. R. Geosci., 337, 1415–1420, https://doi.org/10.1016/j.crte.2005.09.002, 2005.

Pearce, J. A.: Role of the sub-continental lithosphere in magma genesis at active continental margins, in: Continental Basalts and Mantle Xenoliths, edited by: Hawkesworth, C. J. and Norry, M. J., 230–249, Shiva Publishing, Nantwich, UK, 1983.

Pearce, J. A., Harris, N. B. W., and Tindle, A. G.: Trace element discrimination diagrams for the tectonic interpretation of granitic rocks, J. Petrol., 25, 956–983, https://doi.org/10.1093/petrology/25.4.956, 1984.

Pearce, J. A., Kempton, P. D., Nowell, G. M., and Noble, S. R.: Hf-Nd element and isotope perspective on the nature and provenance of mantle and subduction components in Western Pacific arc-basin systems, J. Petrol., 40, 1579 – 1611, https://doi.org/10.1093/petroj/40.11.1579, 1999.

Pearce, J. A. Peate, D. W.: Tectonic implications of the composition of volcanic arc magmas, Annual Review of Earth and Planetary Sciences, 23, 251–285, https://doi.org/10.1146/annurev.ea.23.050195.001343, 1995.

Putirka, K. D.: Thermometers and barometers for volcanic systems, Rev. Mineral. Geochem., 69, 61 – 120, https://doi.org/10.2138/rmg.2008.69.3, 2008.

https://doi.org/10.5194/egusphere-2026-5465
Preprint. Discussion started: 22 September 2026


Putirka, K. D., Mikaelian, H., Ryerson, F., and Shaw, H.: New clinopyroxene-liquid thermobarometers for mafic, evolved, and volatile-bearing lava compositions, with applications to lavas from Tibet and the Snake River Plain, Idaho, Am. Mineral., 88, 1542–1554, https://doi.org/10.2138/am-2003-1017, 2003.

Qiu, L., Li, X., Li, X. W., Yan, D. P., Ren, M. H., Zhang, L. L., and Cheng, G. S.: Petrogenesis of Early Cretaceous intermediate to felsic rocks in Shanghai, South China: Magmatic response to Paleo-Pacific plate subduction, Tectonophysics, 838, 229469, https://doi.org/10.1016/j.tecto.2022.229469, 2022.

Qi, L., Hu, J., and Grégoire, D. C.: Determination of trace elements in granites by inductively coupled plasma mass spectrometry, Talanta, 51, 507–513, https://doi.org/10.1016/S0039-9140(99)00318-5, 2000.

Qiu, J. S., Xiao, E., Hu, J., Xu, X. S., Jiang, S. Y., and Li, Z.: Petrogenesis of highly fractionated I-type granites in the coastal area of northeastern Fujian Province: Constraints from zircon U-Pb geochronology, geochemistry and Nd-Hf isotopes, Acta Petrol. Sin., 24, 2468–2484, 2008.

Rapp, R. P. and Watson, E. B.: Dehydration melting of metabasalt at 8-32 kbar: Implications for continental growth and crust-mantle recycling, J. Petrol., 36, 891–931, https://doi.org/10.1093/petrology/36.4.891, 1995.

Richards, J. P.: High-Sr/Y arc magmas and porphyry Cu ± Mo ± Au deposits: Just add water, Econ. Geol., 106, 1075-1081, https://doi.org/10.2113/econgeo.106.7.1075, 2011.

Rickwood, P. C.: Boundary lines within petrologic diagrams which use oxides of major and minor elements, Lithos, 22, 247-263, https://doi.org/10.1016/0024–4937(89)90028-5, 1989.

Ridolfi, F., Renzulli, A., and Puerini, M.: Stability and chemical equilibrium of amphibole in calc-alkaline magmas: An overview, new thermobarometric formulations and application to subduction-related volcanoes, Contrib. Mineral. Petrol., 160, 45–66, https://doi.org/10.1007/s00410-009-0465-7, 2010.

Rogers, G. and Hawkesworth, C. J.: A geochemical traverse across the North Chilean Andes: Evidence for crust generation from the mantle wedge, Earth Planet. Sci. Lett., 91, 271–285, https://doi.org/10.1016/0012-821X(89)90003-4, 1989.

Rollinson, H. R.: Using Geochemical Data: Evaluation, Presentation, Interpretation, Longman Scientific & Technical, Harlow, 352 pp., 1993.

Rudnick, R. L. and Gao, S.: Composition of the continental crust, in: Treatise on Geochemistry, Vol. 3, The Crust, edited by Rudnick, R. L., Elsevier-Pergamon, Oxford, 1–64, https://doi.org/10.1016/B0-08-043751-6/03016-4, 2003.

Schiano, P., Monzier, M., Eissen, J. P., Martin, H., and Koga, K. T.: Simple mixing as the major control of the evolution of volcanic suites in the Ecuadorian Andes, Contrib. Mineral. Petrol., 160, 297–312, https://doi.org/10.1007/s00410-009-0478-2, 2010.

Schmidt, M. W. and Jagoutz, O.: The global systematics of primitive arc melts, Geochem. Geophys. Geosyst., 18, 2817–2854, https://doi.org/10.1002/2016GC006699, 2017.

Shen, L.W., Yu, J. H., O'Reilly, S. Y., and Griffin, W. L.: Tectonic switching of Southeast China in the Late Paleozoic, J. Geophys. Res.-Sol. Ea., 123, 8508-8526, https://doi.org/10.1029/2018JB015520, 2018.

Shu, L. S., Yao, J. L., Wang, B., Faure, M., Charvet, J., and Chen, Y.: Neoproterozoic plate tectonic process and Phanerozoic geodynamic evolution of the South China Block, Earth-Sci. Rev., 216, 103596, https://doi.org/10.1016/j.earscirev.2021.103596, 2021.

Shu, L. S., Zhou, X. M., Deng, P., and Zhu, W. B.: Mesozoic–Cenozoic basin features and evolution of Southeast China, Acta Geol. Sin., 81, 573–586, 2007.

Shu, L. S., Zhou, X. M., Deng, P., Wang, B., Jiang, S. Y., Yu, J. H., and Zhao, X. X.: Mesozoic tectonic evolution of the Southeast China Block: New insights from basin analysis, J. Asian Earth Sci., 34, 376 – 391, https://doi.org/10.1016/j.jseaes.2008.06.004, 2009.

Sisson, T. W. and Grove, T. L.: Experimental investigations of the role of $H_2O$ in calc-alkaline differentiation and subduction zone magmatism, Contrib. Mineral. Petrol., 113, 143–166, https://doi.org/10.1007/BF00283225, 1993.

Sun, W. D., Ling, M. X., Yang, X. Y., Fan, W. M., Ding, X., and Liang, H. Y.: Ridge subduction and porphyry copper–gold mineralization: An overview, Sci. China Earth Sci., 53, 475–484, https://doi.org/10.1007/s11430-010-0024-0, 2010.

Sun, S. S. and McDonough, W. F.: Chemical and isotopic systematics of oceanic basalts: Implications for mantle composition and processes, Geol. Soc. Lond. Spec. Publ., 42, 313 – 345, https://doi.org/10.1144/GSL.SP.1989.042.01.19, 1989.

Trail, D., Watson, E. B., and Tailby, N. D.: The oxidation state of Hadean magmas and implications for early Earth's atmosphere, Nature, 480, 79–82, https://doi.org/10.1038/nature10655, 2011.

Turner, S., Wilde, S., Wörner, G., Schaefer, B., and Lai, Y. J.: An andesitic source for Jack Hills zircon supports onset of plate tectonics in the Hadean, Nat. Commun., 11, 1241, https://doi.org/10.1038/s41467-020-14857-1, 2020.

Uchida, E., Endo, S., and Makino, M.: Relationship between solidification depth of granitic rocks and formation of hydrothermal ore deposits, Resour. Geol., 57, 47–56, https://doi.org/10.1111/j.1751-3928.2006.00004.x, 2007.

Wang, S., Zhang, D., Wu, G. G., Vatuva, A., Di, Y. J., Yan, P. C., Feng, H. B., and Ma, S.: Late Paleozoic to Mesozoic extension in southwestern Fujian Province, South China: Geochemical, geochronological and Hf isotopic constraints from basic-intermediate dykes, Geosci. Front., 8, 529–540, https://doi.org/10.1016/j.gsf.2016.05.005, 2017.

Wang, X. Y., Yang, F. C., Li, W. C., Liu, K., and Zhang, Z. J.: Repeated recharge of mafic magmas and large-scale fluid exsolution facilitate the formation of the giant Siahdik porphyry Cu deposit, western Chagai, Pakistan, Ore Geol. Rev., 192, 107256, https://doi.org/10.1016/j.oregeorev.2026.107256, 2026.

Wang, Z. Y., Zhao, X. L., Yu, S. Y., Li, S. Z., Peng, Y. B., and Liu, Y. J.: Cretaceous granitic intrusions in Fujian Province, Cathaysia Block: Implications for slab rollback and break-off of the Paleo-Pacific plate, J. Asian Earth Sci., 190, 104164, https://doi.org/10.1016/j.jseaes.2019.104164, 2020.

Waters, L. E. and Lange, R. A.: An updated calibration of the plagioclase–liquid hygrometer–thermometer applicable to basalts through rhyolites, Am. Mineral., 100, 2172–2184, https://doi.org/10.2138/am-2015-5232, 2015.

https://doi.org/10.5194/egusphere-2026-5465
Preprint. Discussion started: 22 September 2026


Wei, W., Lin, W., Chen, Y., Faure, M., Ji, W.B., Hou, Q.L., Yan, Q.R., and Wang, Q.C.: Tectonic controls on magmatic tempo in an active continental margin: Insights from the Early Cretaceous syn-tectonic magmatism in the Changle-Nan'ao Belt, South China, J. Geophys. Res.-Solid Earth, 128, e2022JB025973, https://doi.org/10.1029/2022JB025973, 2023.

Wones, D. R.: Significance of the assemblage titanite+magnetite+quartz in granitic rocks, Am. Mineral., 74, 744–749, 1989.

Wones, D. R. and Eugster, H. P.: Stability of biotite: Experiment, theory, and application, Am. Mineral., 50, 1228–1272, 1965.

Wu, F. Y., Yang, J. H., Xu, Y. G., Wilde, S. A., and Walker, R. J.: Destruction of the North China Craton in the Mesozoic, Annu. Rev. Earth Planet. Sci. , 47, 173–195, https://doi.org/10.1146/annurev-earth-053018-060342, 2019.

Xu, X. S., Dong, C. W., Li, W. X., and Zhou, X. M.: Late Mesozoic intrusive complexes in the coastal area of Fujian, SE China: The significance of the gabbro-diorite-granite association, Lithos, 46, 299–315, https://doi.org/10.1016/S0024-4937(98)00087-5, 1999.

Ye, G., Mao, G. Z., Xu, Q. L., Ding, Z. J., Han, Y. C., Zhao, H. J., and Shen, Y.: Petrogenesis of the Early Cretaceous Tietonggou diorite and its geological implications, Minerals, 14, 390, doi:10.3390/min14040390, 2024.

Yuan, H. L., Gao, S., Liu, X. M., Li, H. M., Günther, D., and Wu, F. Y.: Accurate U-Pb age and trace element determinations of zircon by laser ablation-inductively coupled plasma-mass spectrometry, Geostand. Geoanal. Res., 28, 353–370, https://doi.org/10.1111/j.1751-908X.2004.tb00755.x, 2004.

Zeng, R. Y., Allen, M. B., Mao, X. C., Lai, J. Q., Yan, J., and Wan, J. J.: Whole-rock and zircon evidence for evolution of the Late Jurassic high Sr/Y Zhoujiapuzi granite, Liaodong Peninsula, North China Craton, Solid Earth, 13, 1259–1280, https://doi.org/10.5194/se-2021-129, 2022.

Zeng, R. Y., Lai, J. Q., Mao, X. C., Xiao, W. Z., Yan, J., Zhang, C. G., Hu, J. X., and Ai, Q. X.: Petrogenesis and tectonic significance of the Early Devonian lamprophyres and diorites in the Alxa Block, NW China, Geochemistry, 81, 125685, https://doi.org/10.1016/j.chemer.2020.125685, 2021.

Zeng, R. Y., Su, H., Allen, M. B., Shi, H. Y., Du, H. F., Zhang, C. G., and Yan, J.: Petrogenesis of early Paleozoic I-type granitoids in the Longshoushan and implications for the tectonic affinity and evolution of the southwestern Alxa Block, Solid Earth, 16, 179–196, https://doi.org/10.5194/se-16-179-2025, 2025.

Zhang, H. J., Lü, Q. T., Wang, X. L., Han, S. C., Liu, L. J., Gao, L., Wang, R., and Hou, Z. Q.: Seismically imaged lithospheric delamination and its controls on the Mesozoic Magmatic Province in South China, Nat. Commun., 14, 2718, https://doi.org/10.1038/s41467-023-37855-5, 2023.

Zhao, F. Y., Suo, Y. H., Liu, L. J., Cao, X. Z., Li, S. Z., Jiang, S. H., Deng, J. Z., Dai, M. X., Liu, Y., Hu, Y. P., Sheng, S. Z., and Hu, B.: Fine lithospheric structure controlling Meso-Cenozoic tectono-magmatism in the South China Block: Inference from a multidisciplinary analysis, Earth-Sci. Rev., 244, 104524, https://doi.org/10.1016/j.earscirev.2023.104524, 2023.

Zhao, G.C., and Cawood, P. A.: Precambrian geology of China, Precambrian Res., 222-223, 13-54, https://doi.org/10.1016/j.precamres.2012.09.017, 2012.

https://doi.org/10.5194/egusphere-2026-5465
Preprint. Discussion started: 22 September 2026


Zhao, J. H.: Geochronology and geochemistry of mafic rocks in Fujian Province: mantle evolution of southeastern China since the Late Mesozoic, PhD thesis, Institute of Geochemistry, Chinese Academy of Sciences, Guiyang, China, 2004.

Zheng, H. Q., Gong, J. F., Wu, H. X., Deng, H. D., Hao, Y. T., Zhu, K. Y., Yu, Z. Q., Huang, J. K., Chen, H. L., and Yang, S. F.: Latest Early Cretaceous tectonic transition from contraction to large-scale extension in Southeast China: Insights from the magmatism along the Changle-Nan'ao Fault Zone, Lithos, 508–509, 108108, https://doi.org/10.1016/j.lithos.2025.108108, 2025.

Zhou, S. D., Wu, B., and Wang, X. L.: Secular lithospheric delamination controls Late Mesozoic magmatism and basin evolution in South China, Earth Planet. Sci. Lett., 671, 119660, https://doi.org/10.1016/j.epsl.2025.119660, 2025.

Zhou, X. M. and Li, W. X.: Origin of Late Mesozoic igneous rocks in southeastern China: Implications for lithosphere subduction and underplating of mafic magmas, Tectonophysics, 326, 269 – 287, https://doi.org/10.1016/S0040-1951(00)00120-7, 2000.

Zhou, X. M., Sun, T., Shen, W. Z., Shu, L. S., and Niu, Y. L.: Petrogenesis of Mesozoic granitoids and volcanic rocks in South China: A response to tectonic evolution, Episodes, 29, 26–33, https://doi.org/10.18814/epiiugs/2006/v29i1/004, 2006.